PHYSICAL REVIEW D **91,** 095009 (2015)

Stealth QCD-like strong interactions and the $t\bar{t}$ asymmetry

Joachim Brod,[1,*] Jure Drobnak,[2,†] Alexander L. Kagan,[1,‡] Emmanuel Stamou,[3,4,§] and Jure Zupan[1,‖]

[1]*Department of Physics, University of Cincinnati, Cincinnati, Ohio 45221, USA*

[2]*Technische Universität München, TUM Institute for Advanced Study, Lichtenbergstrasse 2a, D-85748 Garching, Germany*

[3]*Department of Particle Physics & Astrophysics, Weizmann Institute of Science, Rehovot 76100, Israel*

[4]*Technische Universität München, Excellence Cluster Universe, Boltzmannstrasse 2, D-85748 Garching, Germany*

(Received 23 August 2014; published 15 May 2015)

We show that a new strongly interacting sector can produce large enhancements of the $t\bar{t}$ asymmetries at the Tevatron. The Standard Model is extended by a new vectorlike flavor triplet of fermions and one heavy scalar, all charged under a hypercolor gauge group $\mathrm{SU}(3)_{\mathrm{HC}}$. This simple extension results in a number of new resonances. The predictions of our model are rather rigid once a small number of UV parameters is fixed, since all the strong dynamics can be directly taken over from our understanding of QCD dynamics. Despite the rather low hypercolor confinement scale of ∼100 GeV, the new strongly interacting sector is stealth. It is shielded from present direct and indirect New Physics searches since the light resonances are QCD singlets, whereas the production of the heavier QCD colored resonances leads predominantly to high-multiplicity final states. Improved searches can potentially be devised using top tagged final states or decays into a small number of hypercolor pions.

DOI: 10.1103/PhysRevD.91.095009 PACS numbers: 12.60.Nz, 14.65.Ha

I. INTRODUCTION

Strongly interacting theories with a low confinement scale, e.g., $f_\pi \lesssim 100$ GeV, are a particularly interesting possibility for new physics in the LHC era, due to the large number of resonances that could be experimentally accessible. In view of the recent discovery of the Higgs-like particle, an interesting framework in which a low confinement scale is motivated by electroweak symmetry breaking is "bosonic technicolor," where the vacuum expectation value of a fundamental Higgs is induced from technicolor (TC) dynamics [1–9], and supersymmetry is introduced to protect the Higgs mass [2,3,6,8,9].

More generally, several classes of strongly interacting theories with a low confinement scale and distinct phenomenologies have been proposed, which are not directly linked to electroweak symmetry breaking. In "hidden valley" models [10,11], the new strongly interacting fermions which undergo confinement are neutral with respect to the Standard Model (SM) interactions, thus effectively hiding their bound states at colliders. In "quirk" models, the confining fermions or quirks are taken to have color or electroweak charges and have masses that are much heavier than the new strong interaction scale [12–18]. They therefore form long stable strings at colliders with exotic signatures that depend on the quirk mass. Finally, in Refs. [19–22] collider signatures of "vectorlike confinement" models were studied, in which the confining "hypercolor quark" masses are small compared to the confinement scale, as in QCD. Variants containing weak scale colored mesons already tend to be ruled out by LHC and Tevatron data.

In this paper we show that potentially enhanced top-quark forward-backward asymmetries ($A_{\mathrm{FB}}^{t\bar{t}}$) at the Tevatron could be a manifestation of a new strong interaction with a low confinement scale that is not directly related to electroweak symmetry breaking. Among the many proposals leading to large asymmetries [23], only a small subset satisfies all flavor constraints without fine-tuning. The t-channel models have new vector or scalar resonances with masses of $\mathcal{O}(200\ \mathrm{GeV})$, transforming nontrivially under flavor symmetries [24–27].

There are two possibilities for flavorful vector fields in a renormalizable theory: either they are fundamental gauge bosons of a flavor symmetry, or they are composite. While theories with light gauged flavor bosons are a logical possibility, flavor constraints could be particularly challenging to satisfy, and they could require a complicated and potentially fine-tuned Higgs sector; see e.g. Refs. [28,29]. We thus explore the second option, which implies a strong interaction confinement scale of ∼100 GeV. Surprisingly, this possibility is not excluded by existing collider searches.

We build an explicit model with a confining hypercolor (HC) gauge group, $\mathrm{SU}(3)_{\mathrm{HC}}$. The hypercolored matter consists of three "light" flavors of vectorlike fermion "HC quarks" that are neutral with respect to the SM gauge

*joachim.brod@uc.edu
†jure.drobnak@tum.de
‡kaganalexander@gmail.com
§emmanuel.stamou@weizmann.ac.il
‖zupanje@ucmail.uc.edu

interactions (they will be identified with the flavors of the ordinary right-handed up quarks), with masses of ∼3–30 GeV lying well below the strong interaction scale, like the u, d, s quarks in QCD. A hallmark of this model is the existence, following confinement, of new SM singlet resonances with masses between 60 and 300 GeV organized in flavor nonets of pseudoscalar, vector, axial-vector, and higher mass resonances. They are the equivalent of the QCD resonances but with HC scale confinement dynamics. There is also a "heavy" flavor-singlet fundamental "HC scalar," $\mathcal{S}$, with a mass of ∼500 GeV lying well above the strong interaction scale. It is an electrically charged QCD triplet which decays before it can hadronize.

Remarkably, while the new states are relatively light and can lead to large changes in the Tevatron $t\bar{t}$ asymmetries, the current LHC and Tevatron searches are not yet sensitive to their production. The reason is that in our model the light HC resonances are color singlets and thus have relatively small cross sections. The only QCD colored new states are the heavier elementary HC scalars that carry both QCD and HC charge. However, their detection is challenging, as their production results in high-multiplicity events, for instance $pp \to n\pi_{\rm HC} + 2j$ with n large, and with the HC pions, $\pi_{\rm HC}$, decaying to two jets.

In the limit of a large mass for the HC scalar $\mathcal{S}$, our model can effectively be thought of as a confining hidden valley model [10,11]. In both cases the composite resonances are not charged under the SM. However, in our case the interaction with the SM is not through a Z' as in Refs. [10,11] but through Yukawa-like interactions involving a HC quark, the HC scalar $\mathcal{S}$, and an ordinary right-handed up quark. Unlike in the case of the hidden valley, the HC pions decay to quark pairs, and we thus have no or very little missing E_T and/or leptons in the events. The second difference between our model and hidden valley models is that the couplings of the new states to the SM are large. Thus, virtual exchanges of these states can lead to observable consequences, such as significant changes to the $t\bar{t}$ asymmetry at the Tevatron.

The two most important New Physics (NP) contributions to the $t\bar{t}$ asymmetry are the exchanges of the HC vector resonance $K^*_{\rm HC}$ and the pseudoscalar resonance $K_{\rm HC}$, by virtue of their flavor off-diagonal couplings to the u and t quarks; see Fig. 1. Our model is thus a realization of the effective t-channel models that have been discussed in the literature, but with both vector and (pseudo)scalar exchanges, rather than only one of these. The K^* acts as the Z' in effective t-channel models [30] and the K as the (pseudo)scalar state [31,32]. At the LHC, the associated production of $K^*_{\rm HC}$ and $K_{\rm HC}$ in the $t\bar{t}j$ final state is also important for reducing the charge asymmetry $A_{\rm C}$, as stressed for Z' models in Ref. [33] (for next-to-leading order (NLO) see also Ref. [34]). To avoid other constraints, e.g. bounds on top-jet resonance production at the LHC, the branching ratio of the decay $K^*_{\rm HC} \to q\bar{t}$ should be of order 25%. This is achieved naturally in our model since the $K^*_{\rm HC}$ decays dominantly into pairs of pseudoscalar mesons, in analogy with the decay $K^* \to K\pi$ in QCD.

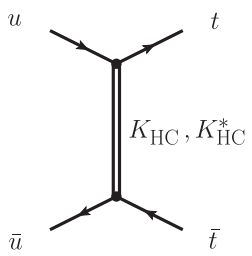

FIG. 1. Feynman diagram generating a contribution to the $t\bar{t}$ asymmetry via a t-channel exchange of K and K^* resonances.

Note that, in order to have large $t\bar{t}$ asymmetry, a relatively large Yukawa coupling between the HC and the SM fields is needed. For the considered values of the Yukawa couplings, the two-loop renormalization-group equations (RGEs) suggest the existence of a strongly interacting UV fixed point. Under this assumption our theory can thus be extended to arbitrarily high scales in the UV.

The paper is organized as follows. In Sec. II we introduce our simple extension of the Standard Model, in Sec. III we discuss in detail the mass spectra and interactions of the resulting resonances, while Sec. IV covers the LHC and Tevatron phenomenology, including the $t\bar{t}$ asymmetries. Section V covers precision electroweak constraints and perturbations of the Higgs properties. Future searches are covered in Sec. VI, including a brief discussion of the lightest HC baryon and dark matter direct detection experiments. Our conclusions are collected in Sec. VII. Three Appendixes contain further details on translating information from QCD to the parameters of the effective HC interaction Lagrangians.

II. SETUP

QCD provides the prototype for a confining theory with a spectrum that contains flavorful vector mesons. Using QCD as a guide, we introduce an asymptotically free confining $\mathrm{SU}(N)_{\rm HC}$ HC gauge group. The anomaly-free matter content consists of the SM and three copies of vectorlike hypercolor quarks $\mathcal{Q}_{Li}, \mathcal{Q}_{Ri}$ $(i = 1, 2, 3)$ and a flavor-singlet hypercolor scalar $\mathcal{S}$, transforming as

$$\begin{aligned} \mathcal{Q}_{Li} &\sim (N, 1, 1, a), \\ \mathcal{Q}_{Ri} &\sim (N, 1, 1, a), \\ \mathcal{S} &\sim (\bar{N}, 3, 1, b), \end{aligned} \tag{1}$$

with respect to the gauge symmetry $\mathrm{SU}(N)_{\rm HC} \times \mathrm{SU}(3)_{\rm C} \times \mathrm{SU}(2)_L \times \mathrm{U}(1)_Y$. The hypercharge assignments satisfy $a + b = 2/3$. The choice $a = 0, b = 2/3$ is phenomenologically favored, as we will see below, and will be used in the main part of the paper.

The most general renormalizable NP Lagrangian is given by

$$-\mathcal{L}_{\rm NP} = (\mathbf{h}_{ij}\bar{u}_{Ri}\mathcal{Q}_{Lj}\mathcal{S} + \text{H.c.}) + \mathbf{m}_{\mathcal{Q}ij}\bar{\mathcal{Q}}_i\mathcal{Q}_j + \mu_{\mathcal{S}}^2\text{Tr}(\mathcal{S}^\dagger\mathcal{S}) + \lambda_1\text{Tr}(\mathcal{S}^\dagger\mathcal{S})^2 + \lambda_2\text{Tr}(\mathcal{S}^\dagger\mathcal{S}\mathcal{S}^\dagger\mathcal{S}) + \lambda_H H^\dagger H\text{Tr}(\mathcal{S}^\dagger\mathcal{S}), \quad (2)$$

plus the kinetic energy terms, where H is the SM Higgs and u_{Ri} the SM right-handed (RH) up quarks. The quartic interactions are not relevant for this work. However, we do require that the couplings $\lambda_{1,2}, \lambda_H$ do not lead to a non-vanishing vacuum expectation value (vev) for $\mathcal{S}$. The total mass of the scalar $\mathcal{S}$ is $m_{\mathcal{S}}^2 = \mu_{\mathcal{S}}^2 + \lambda_H v^2/2$, where $v/\sqrt{2}$ is the SM Higgs vev. In the context of naturalness, we can imagine that the scalar $\mathcal{S}$ is actually composite, or we can invoke supersymmetry above $O(1\ \text{TeV})$ to protect its mass.

In the absence of Yukawa interactions and HC quark masses, the theory respects the global symmetry group $\text{G}_\text{F} = \text{U}(3)_{U_R} \times \text{U}(3)_{D_R} \times \text{U}(3)_{Q_L}$, like the SM. Under the $\text{U}(3)_{U_R}$ symmetry, both (u_{R1}, u_{R2}, u_{R3}) and $(\mathcal{Q}_1, \mathcal{Q}_2, \mathcal{Q}_3)$ transform as flavor triplets. In the SM the main sources of flavor breaking are the top and bottom Yukawa couplings that break G_F to its subgroup

$$\text{H}_\text{F} = \text{U}(2)_{U_R} \times \text{U}(2)_{D_R} \times \text{U}(2)_{Q_L} \times \text{U}(1)_3. \quad (3)$$

Here, we assume that the NP interactions also respect H_F; i.e. the new Yukawa couplings and mass terms are of the form

$$\mathbf{h} = \text{diag}(h_1, h_1, h_3), m_{\mathcal{Q}} = \text{diag}(m_{\mathcal{Q}1}, m_{\mathcal{Q}1}, m_{\mathcal{Q}3}). \quad (4)$$

The breaking of H_F in the SM is due to the light-quark Yukawa couplings and the CKM mixing angles and is thus small. We will assume that this breaking continues to be small in our model. The approximate $\text{U}(2)_{U_R}$ symmetry protects against dangerous flavor violation. We assume that its breaking is small, e.g. of minimally flavor violating type. Thus, new contributions to D_0–$\bar{D}_0$ mixing as well as single and same-sign top production are negligible.[1]

We stress the following:

(i) The fact that the hypercolor matter only couples to the RH up quarks is due to the choice of representations. For example, had we chosen a hypercharge assignment such that $a + b = -1/3$ in Eq. (1), the hypercolor quarks $\mathcal{Q}_i$ would only couple to the RH SM down quarks. Alternatively, they could couple to the left-handed (LH) quarks if the $\mathcal{Q}_i$'s were $\text{SU}(2)_L$ doublets.

(ii) Our setup is potentially compatible with generation of the quark mass and mixing hierarchies via spontaneous breaking of a horizontal non-Abelian symmetry in the UV, e.g. SU(3), SU(2), or discrete non-Abelian groups.[2] In such a scenario, the $\text{U}(2)_{U_R}$ global symmetry of the hypercolor sector would be a consequence of the underlying horizontal symmetry, under which *all of the quarks* transform.

(iii) The flavor structure of the resonance mass spectrum, to be discussed below, could provide a hint for the existence of such a fundamental horizontal symmetry in the UV (see also Ref. [35]).

III. HYPERCOLOR RESONANCES AND INTERACTIONS

To make use of the available information on nonperturbative QCD dynamics, we take the HC gauge group to be $\text{SU}(3)_\text{HC}$. The HC condensates, resonance masses, and couplings are estimated via naive dimensional analysis (NDA), vector-meson dominance (VMD), and/or scaling from QCD. The $\mathcal{Q}$ and $\mathcal{S}$ masses are taken to satisfy $m_{\mathcal{Q}_i} \ll \Lambda_\chi$ and $m_{\mathcal{S}} \gtrsim \Lambda_\chi$, where $\Lambda_\chi \sim 4\pi f_\pi$ is the HC chiral symmetry breaking scale (the motivation for this choice is given below, in Sec. III C). We also introduce the scale $\Lambda_\text{HC} \sim \mathcal{O}(\text{few}) f_\pi$, which is the equivalent of Λ_QCD in QCD. The phenomenology that we are interested in is dominated by the lowest-lying HC resonances. We thus keep the following resonances in the description:

(i) the flavor octet of pseudo-Goldstone pseudoscalar resonances, π^a_HC,

(ii) the set of lowest-lying vector, ρ^a_HC, and axial vector, $a^a_{1,\text{HC}}$, flavor nonet resonances.

In principle one could include additional HC resonances, e.g. the ${}^1P_1$ axial-vector multiplet [in QCD it contains the $b_1(1235)$ and K_{1B}]. For simplicity, however, we ignore them in this work. Our notation is directly borrowed from QCD: π_HC is thus the equivalent of π in QCD, etc. To shorten the notation, we will often drop the HC subscript. For this reason in this paper the QCD states always carry a QCD subscript or superscript.

To illustrate the effect on $t\bar{t}$ production and other collider and low-energy observables, we consider a benchmark in the parameter space. The benchmark resonance masses and decay widths are given in Table I. The underlying UV parameters, as well as resonance couplings and decay constants, are listed in Table II. The determination of the resonance properties is described in detail below.

A. Pseudo-Nambu–Goldstone bosons

In the $\text{U}(3)_{U_R}$ symmetric limit, the $\mathcal{Q}_i$ form equal condensates, $\langle\bar{\mathcal{Q}}\mathcal{Q}\rangle \neq 0$, which break the HC sector chiral symmetry to the diagonal subgroup, $\text{SU}(3)_L \times \text{SU}(3)_R \to \text{SU}(3)_V$. This gives rise to a flavor

[1] Alternatively, one could entertain the possibility of an Abelian $\text{U}(1)_\text{H}$ horizontal symmetry, with diagonal but fully nondegenerate $\mathbf{h}$ and $m_{\mathcal{Q}}$ entries.

[2] Again, Abelian U(1) symmetries provide a possible alternative.

octet of pseudo-Nambu–Goldstone bosons (pNGBs) $\pi^a_{\rm HC}$ ($a = 1, \ldots, 8$). In NDA, $\Lambda_\chi \sim 4\pi f_\pi^{\rm HC}$ and

$$\langle \bar{\mathcal{Q}}\mathcal{Q}\rangle \sim 4\pi (f_\pi^{\rm HC})^3, \qquad m^2_{\pi^a} \sim 8\pi f_\pi^{\rm HC} m_{\mathcal{Q}}, \tag{5}$$

where $f_\pi^{\rm HC}$ is the HC-pion decay constant,

$$\langle \pi^a | \bar{\mathcal{Q}} T^a \gamma_\mu \gamma_5 \mathcal{Q}|0\rangle = -i f_\pi^{\rm HC} p_\mu. \tag{6}$$

The flavor octet Gell-Mann matrices are normalized as $\mathrm{Tr}[T^a T^b] = \delta^{ab}/2$. For $\langle \bar{\mathcal{Q}}\mathcal{Q}\rangle$ we use the recent lattice determination of the QCD condensate [36], which gives $29.8(f_\pi^{\rm QCD})^3$, instead of the NDA estimate $4\pi(f_\pi^{\rm QCD})^3$ in Eq. (5) (in our convention $f_\pi^{\rm QCD} \simeq 92$ MeV). Similarly, for the pion mass, we take 2×29.8 instead of the factor 8π in Eq. (5). Requiring the vector resonances to have masses in the phenomenologically favored range of approximately 200 GeV fixes $f_\pi^{\rm HC} \simeq 20$ GeV, cf. Eq. (7) below. Thus, for $m_{\mathcal{Q}} \sim \mathcal{O}(10)$ GeV the masses of the pseudoscalars are $m_\pi^{\rm HC} \sim \mathcal{O}(100)$ GeV.

In our benchmark we take $m_{\mathcal{Q}3} \sim f_\pi$ and $m_{\mathcal{Q}1} \sim m_{\mathcal{Q}3}/10$. The flavor-symmetry breaking, $m_{\mathcal{Q}_1} \neq m_{\mathcal{Q}_3}$, leads to mass splitting between the $\pi \sim [\bar{\mathcal{Q}}_{1,2}\mathcal{Q}_{1,2}]$, $K \sim [\bar{\mathcal{Q}}_{1,2}\mathcal{Q}_3]$, and $\eta \sim [\bar{\mathcal{Q}}_1\mathcal{Q}_1 + \bar{\mathcal{Q}}_2\mathcal{Q}_2 - 2\bar{\mathcal{Q}}_3\mathcal{Q}_3]$, where the valence-quark content is given in square brackets. Details of the evaluation of their masses are given in Appendix A. The pseudoscalar mass spectrum also contains a heavier $\eta'_{\rm HC}$ flavor singlet. The mass of the $\eta'_{\rm HC}$ is $m_{\eta'} \sim \Lambda_\chi$, i.e. $m_{\eta'} \sim \mathcal{O}(250)$ GeV. The $\eta'_{\rm HC}$ has flavor diagonal couplings to the SM quarks. For the light quarks, these are suppressed by the light-quark masses. The $\eta'_{\rm HC}$ thus has a negligible impact on $t\bar{t}$ and dijet phenomenology, as well as on the vector decay widths (due to its large mass). As such it can be omitted from our discussion. For simplicity we also neglect "$\eta - \eta'$" mixing.

B. Vectors and axial vectors

As in QCD, the $[\bar{\mathcal{Q}}\mathcal{Q}]$ bound states give rise to vector and axial-vector resonances that are flavor nonets. We denote the lowest-lying states by $\rho^a_{\rm HC}$ and $a^a_{1\,\rm HC}$ ($a = 1, \ldots, 9$), respectively. Here, $\rho^9_{\rm HC}$ and $a^9_{1\,\rm HC}$ are the flavor-singlet states. Sometimes we will also use the generic notation of V and A for vector and axial-vector mesons.

We first discuss the properties of these resonances in the flavor-symmetric limit. The masses and decay constants can be estimated via the approximate scaling relations

$$\frac{f_\pi^{\rm HC}}{f_\pi^{\rm QCD}} \sim \frac{f^{\rm HC}_{\rho(a_1)}}{f^{\rm QCD}_{\rho(a_1)}} \sim \frac{m^{\rm HC}_{\rho(a_1)}}{m^{\rm QCD}_{\rho(a_1)}}, \tag{7}$$

with $f_\pi^{\rm QCD} \simeq 92$ MeV. The $\rho^a_{\rm HC}$ and $a^a_{1\,\rm HC}$ decay constants are defined as

$$\langle \rho^a_{\rm HC} | \bar{\mathcal{Q}} T^a \gamma_\mu \mathcal{Q}|0\rangle = -i f_\rho^{\rm HC} m_\rho^{\rm HC} \epsilon_\mu, \tag{8}$$

$$\langle a^a_{1\,\rm HC} | \bar{\mathcal{Q}} T^a \gamma_\mu \gamma_5 \mathcal{Q}|0\rangle = -i f^{\rm HC}_{a_1} m^{\rm HC}_{a_1} \epsilon_\mu, \tag{9}$$

where the flavor-singlet matrix $T^9 \equiv I_{3\times3}/\sqrt{6}$. In QCD, the ρ decay constant is $f_\rho^{\rm QCD} \simeq 148$ MeV [37]. The a_1 decay constant $f^{\rm QCD}_{a_1}$ is not well known. For example, a light-cone sum-rule determination yields $f^{\rm QCD}_{a_1} \simeq 168$ MeV [38]. Isgur *et al.* [39] made a phenomenological determination from the $\tau^+ \to \nu_\tau \pi^+\pi^+\pi^-$ branching ratio. Rescaling their result to the current branching ratio from the Particle Data Group [40] would yield $f_{a_1} \simeq 152$ MeV. (Note that the quoted values of the ρ and a_1 decay constants have been reduced by a factor $1/\sqrt{2}$ to conform to our normalization for f_π.) As an example, taking the sum-rule value for $f^{\rm QCD}_{a_1}$, the scaling relations would imply

$$\frac{f_\rho^{\rm HC}}{m_\rho^{\rm HC}} \sim 0.19, \qquad \frac{f^{\rm HC}_{a_1}}{m^{\rm HC}_{a_1}} \sim 0.13, \tag{10}$$

in accord with Weinberg's sum rules that require $f^{\rm HC}_{a_1}/m^{\rm HC}_{a_1} < f_\rho^{\rm HC}/m_\rho^{\rm HC}$. Eq. (7) also implies

$$\frac{m^{\rm HC}_{a_1}}{m_\rho^{\rm HC}} \sim 1.6. \tag{11}$$

Motivated by $A_{\rm FB}^{t\bar{t}}$, we consider $m_\rho^{\rm HC} \sim 200$ GeV, corresponding to $f_\pi^{\rm HC} \sim 20$ GeV.

In the flavor-symmetric limit, the flavor octet ρ^a decays primarily to pairs of HC pions, with the decay width

$$\Gamma_{\rho\to\pi\pi} = \frac{g^2_{\rho\pi\pi}}{32\pi} m_\rho \left(1 - \frac{4m_\pi^2}{m_\rho^2}\right)^{\frac{3}{2}}, \tag{12}$$

where $g_{\rho\pi\pi}$ is the $\rho\pi\pi$ coupling in

$$\mathcal{L}_{\rho\pi\pi} = -g_{\rho\pi\pi} f_{abc} \rho^a_\mu \pi^b \partial^\mu \pi^c. \tag{13}$$

The VMD estimate

$$g_{\rho\pi\pi} \simeq m_\rho / f_\rho \tag{14}$$

agrees with the NDA estimate $g_{\rho\pi\pi} \sim \mathcal{O}(4\pi)$ within a factor of ~2. In QCD the VMD prediction is only 16% smaller than the measured value. Based on the above, we can expect $\Gamma_\rho/m_\rho \sim \mathcal{O}(10\%)$.

Flavor-symmetry breaking due to $m_{\mathcal{Q}1} \neq m_{\mathcal{Q}3}$ splits the $\rho \sim [\bar{\mathcal{Q}}_{1,2}\mathcal{Q}_{1,2}]$ and $K^* \sim [\bar{\mathcal{Q}}_{1,2}\mathcal{Q}_3]$ masses, as well as the corresponding a_1 and K_1 masses. In general, g_{VPP} ($= g_{\rho\pi\pi}$ in the flavor-symmetric limit) now also depends on the vector and pseudoscalar flavors. Motivated by QCD, we allow for $\mathcal{O}(10\%)$ flavor breaking. The flavor breaking also leads to "$\omega - \phi$" mixing as well as its axial-vector analog. We denote the deviation from ideal vector-meson mixing by the angle $\theta_V^{\rm id}$, so that the relation between the mass eigenstates $V_{L,H}$ and the ideally mixed states,

TABLE I. The spectrum of the HC resonances for our benchmark.

HC resonance	Mass	Decay width
$\pi_{\rm HC}$	62 GeV	$4.0\times10^{-7}m_\pi$
$K_{\rm HC}$	143 GeV	$5.5\times10^{-7}m_K$
$\eta_{\rm HC}$	161 GeV	$1.3\times10^{-7}m_\eta$
$\rho_{\rm HC}$	177 GeV	$0.059m_\rho$
$K^*_{\rm HC}$	211 GeV	$0.002m_{K^*}$
$V_H[\phi_{\rm HC}]$	242 GeV	$8.0\times10^{-7}m_{V_H}$
$V_L[\omega_{\rm HC}]$	180 GeV	$0.001m_{V_L}$
$a_1^{\rm HC}$	273 GeV	$0.23m_{a_1}$
$K_1^{\rm HC}$	295 GeV	$0.057m_{K_1}$
$f_1^{\rm HC}$	280 GeV	$0.002m_{f_1}$
$f_1{}'^{\rm HC}$	320 GeV	$3.2\times10^{-5}m_{f_1'}$

$$|V_{12}\rangle=\frac{1}{\sqrt{2}}(|\bar{\mathcal{Q}}_1\mathcal{Q}_1\rangle+|\bar{\mathcal{Q}}_2\mathcal{Q}_2\rangle),\qquad |V_3\rangle=|\bar{\mathcal{Q}}_3\mathcal{Q}_3\rangle, \tag{15}$$

is given by

$$\begin{pmatrix}|V_L\rangle\\|V_H\rangle\end{pmatrix}=\begin{pmatrix}\cos\theta_V^{\rm id}&\sin\theta_V^{\rm id}\\-\sin\theta_V^{\rm id}&\cos\theta_V^{\rm id}\end{pmatrix}\begin{pmatrix}|V_{12}\rangle\\-|V_3\rangle\end{pmatrix}, \tag{16}$$

and similarly for the axial-vector mixing angle $\theta_A^{\rm id}$, with $V_{L,H}\to A_{L,H}$ and $V_{12,3}\to A_{12,3}$. Frequently, we will also employ QCD inspired notation for the mass eigenstates, i.e. $V_L=\omega_{\rm HC}$, $V_H=\phi_{\rm HC}$, and $A_L=f_1^{\rm HC}$, $A_H=f_1'^{\rm HC}$. Since we do not include the ${}^1P_1$ resonances, there is no equivalent of the K_{1A}-K_{1B} mixing in our simplified formalism. In particular, we identify the $K_1^{\rm HC}$ in Table I with the equivalent of the $K_{1A}^{\rm QCD}$ in QCD.

Given $m_{\mathcal{Q}_1}$ and $m_{\mathcal{Q}_3}$, we determine the vector and axial-vector masses as well as the mixing angles $\theta_{V,A}^{\rm id}$ using the simplified quark-model treatment of Ref. [41]. The HC hadronic parameters of this model are obtained by fitting to the QCD vector and axial-vector meson data and then rescaling to the HC scale, M_χ, as explained in detail in Appendix A. The HC scale is defined to be the ρ mass in the chiral limit,

$$M_\chi\equiv\lim_{m_{\mathcal{Q}_i}\to0}m_\rho. \tag{17}$$

In turn, the π, ρ, and a_1 decay constants are taken to be

$$f_\pi=\frac{M_\chi}{m_\rho^{\rm QCD}}f_\pi^{\rm QCD}, \tag{18}$$

$$f_\rho=\frac{M_\chi}{m_\rho^{\rm QCD}}f_\rho^{\rm QCD}, \tag{19}$$

$$f_{a_1}=\frac{M_\chi}{m_{a_1}^{\rm QCD}}f_{a_1}^{\rm QCD}, \tag{20}$$

where the QCD decay constants that we use are $f_\pi^{\rm QCD}=92$ MeV, $f_\rho^{\rm QCD}=148$ MeV, and $f_{a_1}^{\rm QCD}=168$ MeV.

The $\rho_{\rm HC}$ resonances decay primarily to HC pion pairs, as in QCD, and subdominantly to light-quark pairs; cf. Table III. The $K^*_{\rm HC}$ resonances decay primarily to $K_{\rm HC}+\pi_{\rm HC}$ pairs, as in QCD. Their subdominant decays to $t+$light-quark pairs have a branching ratio of $\approx30\%$, as explained in Sec. IV C. The fact that the $K^*_{\rm HC}\to t+$jet decays are subleading is phenomenologically favored and naturally achieved within our model, as already mentioned in the Introduction. In our benchmark both the $\omega_{\rm HC}$ and $\phi_{\rm HC}$ are kinematically forbidden to decay to on-shell $\bar{K}_{\rm HC}K_{\rm HC}$ pairs. Therefore, their dominant decays are to SM quarks with very narrow decay widths; cf. Table I.

For the axial-vector meson decay widths, we use the model of Ref. [42], where a global SU(3) flavor symmetry is used for the matrix elements, but the phenomenologically more important effect of flavor-symmetry breaking in the phase space of the final states is kept. A hadronic parameter, $\tilde{F}_{\rm QCD}$, obtained from the fit to the $A\to PV$ decay widths in QCD [42] is rescaled to $\tilde{F}_{\rm HC}$ in order to obtain the corresponding HC decay widths. See Appendix C and Eq. (C12) for details. The HC a_1 state decays predominantly to $\rho_{\rm HC}\pi_{\rm HC}$ pairs, yielding a large decay width, $\Gamma_{a_1}\simeq0.2m_{a_1}$. The branching ratio into light-quark pairs is small, $\mathcal{O}(\text{few}\%)$. The HC K_1 resonance decays predominantly to $K^*_{\rm HC}\pi_{\rm HC}$ pairs, yielding $\Gamma_{K_1}\simeq0.05m_{K_1}$. The $K_1\to u,c+t$ branching ratio is of $\mathcal{O}(5\%$–$10\%)$. In our benchmark the decays of the HC $f_1(=A_L)$ and $f_1'(=A_H)$ to $K_{\rm HC}K^*_{\rm HC}$ pairs are

TABLE II. The UV parameters for the benchmark point (left two columns), the resulting HC resonance couplings (middle two columns), and the HC decay constants (last two columns).

Parameter	Value	Parameter	Value	Parameter	Value
M_χ [GeV]	171	g_ρ	4.88	f_π	20.4 GeV
$m_{\mathcal{Q}_1}$ [GeV]	3.1	$g_{\rho\pi\pi}$	4.88	f_ρ	32.6 GeV
$m_{\mathcal{Q}_3}$ [GeV]	30.5	g_{a_1}	6.73	f_{a_1}	37.1 GeV
$m_{\mathcal{S}}$ [GeV]	520	g_{V_o}	12.5	$f_{u',c'}$	53.5 GeV
h_1	2.0	g_{V_s}	5.10	$f_{t'}$	52.4 GeV
h_3	4.2	g_A	1.26		

TABLE III. Table of the dominant branching ratios of HC vector resonances and their decays into SM quarks.

HC resonance	Channel	Br(%)
$\rho_{\rm HC}$	$\pi\pi$	98.2
	$\bar{u}c,\bar{c}u,\bar{u}u+\bar{c}c$	1.8
$K^*_{\rm HC}$	$K\pi$	68
	$\bar{u}t,\bar{t}u,\bar{c}t,\bar{t}c$	32
$V_H[\phi_{\rm HC}]$	$\bar{u}u+\bar{c}c$	100
$V_L[\omega_{\rm HC}]$	$\bar{u}u+\bar{c}c$	100

kinematically forbidden. Therefore, they are very narrow with their dominant decays being to light-quark pairs.

C. Would-be composite quarks

In our benchmark an on-shell HC scalar $\mathcal{S}$ decays to $u_j\bar{\mathcal{Q}}_j$ pairs well before HC hadronization can occur. In particular, the decay width of the heavy scalar $\mathcal{S}$ is

$$\Gamma_{\mathcal{S}} = \sum_j \Gamma_{\mathcal{S}\to u_j\bar{\mathcal{Q}}_j}, \tag{21}$$

where j runs over $j = 1, 2, 3$. The $\mathcal{S} \to u_j\bar{\mathcal{Q}}_j$ partial decay widths are given by

$$\Gamma_{\mathcal{S}\to u_j\bar{\mathcal{Q}}_j} \simeq m_{\mathcal{S}}\frac{|h_j|^2}{16\pi}, \tag{22}$$

up to phase-space corrections which are at most of $\mathcal{O}(10\%)$. In our benchmark the Yukawa couplings are large ($h_i \sim 2$–4), leading to $\Gamma_{\mathcal{S}} \simeq 0.44 \times m_{\mathcal{S}} \simeq 230$ GeV. The $\mathcal{S}$ therefore decays on a time scale that is much shorter than the HC hadronization time scale, which is governed by $\Lambda_{\rm HC} \sim \mathcal{O}(\text{few}) f_\pi \sim \mathcal{O}(60\text{ GeV})$. Consequently, there are no asymptotic bound states of two heavy HC scalars, $\mathcal{S}\mathcal{S}^*$, or of a HC scalar and a HC quark, $\mathcal{S}\mathcal{Q}_i$. (Had we taken the fundamental scalar to be much lighter, $\mathcal{S}\mathcal{S}^*$ bound states would form and clearly show up as resonances in the differential $t\bar{t}$ spectrum. We are thus led to a consider scalar mass $m_{\mathcal{S}} \gtrsim 0.5$ TeV.)

However, the picture changes for production of the elementary quarks u_{Ri} via their Yukawa couplings to the composite operators $\mathcal{S}\mathcal{Q}_i$. The latter are also isosinglet QCD color triplets with hypercharge $2/3$. The SM right-handed up quarks can then be viewed as an admixture of the elementary u_{Ri} and bound-state $\mathcal{S}\mathcal{Q}_i$ quark fields. Note that in this case the scalar $\mathcal{S}$ has virtuality $\sqrt{s} \equiv (p_{\mathcal{S}}^2)^{1/2}$ lying well below $m_{\mathcal{S}}$. The $\mathcal{S}$ decay width becomes s dependent, being obtained via the substitution $m_{\mathcal{S}} \to \sqrt{s}$ in Eq. (22), including the implicit phase-space factor. Thus, its decay width is suppressed to levels $\lesssim\Lambda_{\rm HC}$, and bound-state $\mathcal{S}\mathcal{Q}_i$ quark fields with virtuality much smaller than their would-be physical mass can form and mix into on-shell u_{Ri}.

To estimate the mixing or partial compositeness of the u_{Ri}, we assume that it is dominated by the lowest pole in the $T\{\mathcal{S}\mathcal{Q}_i(x), \mathcal{S}^*\bar{\mathcal{Q}}_i(0)\}$ two-point function, or equivalently, by the lowest pole in the $\mathcal{S}\mathcal{Q}_i \to \mathcal{S}\mathcal{Q}_i$ scattering S matrix. In the calculation of the mixing, we will treat the lowest pole as an asymptotic state. Formally, this corresponds to taking the limit $h_i \to 0$ in Eq. (22), making $\mathcal{S}$ stable.

The Yukawa couplings induce mass mixing between the would-be composite quarks and the elementary up quarks ($u_i = u, c, t$),

$$\sqrt{2}h_i f_{u_i'}\bar{u}_{Ri}u'_{Li}, \tag{23}$$

where the would-be composite quark decay constants $f_{u_i'}$ are defined as

$$\langle u_i'|\bar{\mathcal{Q}}_i\mathcal{S}^*|0\rangle = \sqrt{2}f_{u_i'}\bar{u}_i'. \tag{24}$$

Here, the $\bar{u}_i'$ are the Dirac spinors.

Since $m_{\mathcal{Q}} \ll m_{\mathcal{S}}$ the would-be composite HC quarks correspond to bound states of a heavy–light-quark system. More precisely, in our benchmarks $m_{\mathcal{S}}$ is $\sim 2\Lambda_{\rm HC}$. Comparing to QCD this corresponds to a heavy–light-quark system with a heavy-quark mass lying somewhere between the charm- and bottom-quark mass. To estimate the $f_{u_i'}$ decay constants, we therefore interpolate between the known light–light and heavy–light vector-meson decay constants in QCD and rescale to the case of HC—see Appendix B, Eq. (B5) in particular, for details.

For the purpose of this discussion, we can take the ordinary 3×3 up-quark mass matrix to be flavor diagonal, neglecting the small misalignment between the weak and up-quark mass bases in the SM. For each generation the mixing between the SM and would-be HC quarks is then described by 2×2 matrices,

$$M_{RL}^i = \begin{pmatrix} m_{u_i} & \sqrt{2}h_i f_{u_i'} \\ 0 & M_{u_i'} \end{pmatrix}, \quad i = 1, 2, 3. \tag{25}$$

Here, m_{u_i} is the ordinary $\mathrm{SU}(2)_L$ breaking quark mass, and $M_{u_i'} \simeq m_{\mathcal{Q}_i} + m_{u_i} + \Lambda_{\rm HC}$ is the mass term for the would-be composite quark [see Eq. (A17)]. The mixing term follows from Eq. (23).

Diagonalization of Eq. (25) yields the mass eigenstates

$$|u_{Ri}\rangle^{\rm phys} = \cos\theta_{Ri}|u_{Ri}\rangle - \sin\theta_{Ri}|u'_{Ri}\rangle, \tag{26}$$

$$|u'_{Ri}\rangle^{\rm phys} = \sin\theta_{Ri}|u_{Ri}\rangle + \cos\theta_{Ri}|u'_{Ri}\rangle, \tag{27}$$

and similarly for the LH mass eigenstates with the replacement $R \to L$. The ordinary u, c, and t quarks are identified with $u_1^{\rm phys}$, $u_2^{\rm phys}$, and $u_3^{\rm phys}$, respectively. Taking $h_i f_{u_i'}$ significantly smaller than $M_{u_i'}$ yields

$$\sin\theta_{Ri} \sim \sqrt{2}h_i\frac{f_{u_i'}}{M_{u_i'}}, \qquad \sin\theta_{Li} \sim \sqrt{2}h_i\frac{f_{u_i'}m_{u_i}}{M_{u_i'}^2}. \tag{28}$$

The RH mixings are substantially larger than the LH ones, which are suppressed by the $M_{u_i'}$. Specifically, for our benchmark we find

$$\sin\theta_{R1} = \sin\theta_{R2} = 0.22, \qquad \sin\theta_{R3} = 0.43, \tag{29}$$

$$\sin\theta_{L1} = \sin\theta_{L2} \approx 0, \qquad \sin\theta_{L3} = 0.10. \tag{30}$$

The couplings of the vector mesons to the would-be composite quarks are given by

$$\mathcal{L} = g_\rho(\bar{u}' T^a \gamma^\mu u')\rho_\mu^a + g_{a_1}(\bar{u}' T^a \gamma^\mu \gamma_5 u') a_{1\mu}^a + \cdots. \quad (31)$$

Here, the u' appear in the interaction basis of Eqs. (23)–(25), and, for simplicity, we have taken flavor-symmetric couplings. The ellipses denote higher-derivative operators. In NDA, both g_ρ and g_{a_1} are $\mathcal{O}(4\pi)$, while the VMD estimates are (see Appendix B)

$$g_\rho \simeq \frac{m_\rho}{f_\rho}, \qquad g_{a_1} \simeq \frac{m_{a_1}}{f_{a_1}}, \quad (32)$$

so that $g_\rho \simeq g_{\rho\pi\pi}$. In the numerics below, we will take them to be equal.

Couplings of the vector mesons to the SM quarks are induced then via the quark mixing in Eq. (26). In the quark-mass basis, these couplings are given by

$$\mathcal{L} = \lambda_{ij}^R \bar{u}_{Ri} \gamma^\mu T_{ij}^a \rho_\mu^a u_{Rj} + (R \to L) + \cdots, \quad (33)$$

where

$$\lambda_{ij}^R = g_\rho \sin\theta_{Ri} \sin\theta_{Rj}, \quad (34)$$

and the ellipses denote terms involving the would-be composite quarks.

The LH quark couplings λ_i^L are obtained by substituting $R \to L$ in Eqs. (33)–(34). The axial-vector meson couplings to quarks follow by substituting $\gamma^\mu \to \gamma^\mu\gamma_5$ and $g_\rho \to g_{a_1}$. The $K^* ut$ coupling λ_{113}^R and the corresponding $K_1 ut$ coupling are phenomenologically important for NP contributions to $t\bar{t}$ production from t-channel HC resonance exchanges. On the other hand, the s-channel contributions from ϕ/ω as well as $f_1/f_1{}'$ exchanges are suppressed by the small $\theta_{V,A}^{\rm id}$ mixing angles. The above couplings also govern the partial decay widths of the vector and axial-vector resonances to quark pairs.

Similarly, the interactions of the HC pions with the SM quarks follow from their couplings to the would-be composite quarks,

$$\mathcal{L} = \frac{g_A}{f_\pi}(\bar{u}'_{Ri} T_{ij}^a \partial\pi^a u'_{Rj} - \bar{u}'_{Li} T_{ij}^a \partial\pi^a u'_{Lj}) + \cdots, \quad (35)$$

where the ellipses again denote higher-derivative operators. In NDA $g_A \sim \mathcal{O}(1)$, consistent with the QCD nucleon-pion axial coupling $g_A^{\rm QCD} \simeq 1.26$. Ignoring the spin structure, as warranted in the heavy-scalar limit, one can also compare g_A with the QCD $B^* B\pi$ and $D^* D\pi$ couplings, which are also $\mathcal{O}(1)$ (i.e. $\hat{g} \sim 0.6$–0.7 [43–45]).

Changing to the physical quark basis, the Lagrangian is given by

$$\mathcal{L} = \frac{g_A}{f_\pi} \sin\theta_{Ri} \sin\theta_{Rj} \bar{u}_{Ri} T_{ij}^a \partial\pi^a u_{Rj} - (R \to L), \quad (36)$$

where we do not show the terms that involve would-be HC quarks. Integrating by parts and using the Dirac equation, Eq. (36) is equivalent on the quark-mass shell to

$$\mathcal{L} \simeq \frac{ig_A}{f_\pi} \sin\theta_{Ri} \sin\theta_{Rj} m_{u_j} \bar{u}_{Ri} T_{ij}^a \pi^a u_{Lj} + \text{H.c.} - (\text{R} \to \text{L}). \quad (37)$$

We see that the only significant contribution is proportional to m_t. Thus, production of $t\bar{t}$ pairs receives important contributions from t-channel K exchange. In contrast, s-channel contributions are suppressed by the light-quark masses.

The couplings in Eq. (37) are also responsible for pion decays to quark pairs, e.g. $\pi \to 2j$, $K \to jt^*$. The π^a decay widths are given by

$$\frac{\Gamma_{\pi^a \to \bar{u}_i u_j}}{m_{\pi^a}} = \frac{g_A^2 N_c}{16\pi} \frac{(m_{u_j}^2 + m_{u_i}^2)}{f_\pi^2} T_{ij}^a T_{ji}^a \sin^2\theta_{Ri} \sin^2\theta_{Rj}, \quad (38)$$

where $a = 1, 2, 3$, and we do not write down terms further suppressed by the light-quark masses. While the decay widths are narrow due to light-quark mass suppression, they do not lead to displaced vertices since they correspond to decay lengths of tens of nanometers.

IV. TEVATRON AND LHC PHENOMENOLOGY

Next, we assess the effect of the new HC sector on the $t\bar{t}$ production cross sections and asymmetries at the Tevatron and the LHC. The relevant measurements and the corresponding SM predictions are collected in Tables IV and V. As an example we take the benchmark set of parameters introduced in the previous section. It has been chosen to demonstrate that our model can easily yield anomalously large $A_{\rm FB}^{t\bar{t}}$ asymmetries, while satisfying the remaining $t\bar{t}$ constraints. We also show that the benchmark passes the Tevatron and LHC dijet tests that often invalidate models addressing the Tevatron $A_{\rm FB}^{t\bar{t}}$ anomalies. Cross sections for the production of new resonances that are present in our model are evaluated, and the most promising signals are identified. In Sec. V we will discuss another class of constraints, namely electroweak-precision tests, including atomic-parity violation.

A. The top-antitop asymmetries: Experimental review

The CDF and D0 experiments at the Tevatron have measured various partonic level asymmetries in $p\bar{p} \to t\bar{t}$. One of these is the inclusive asymmetry,

$$A_{\rm FB} \equiv \frac{N(\Delta y > 0) - N(\Delta y < 0)}{N(\Delta y > 0) + N(\Delta y < 0)}, \quad (39)$$

where $\Delta y = y_t - y_{\bar{t}}$ is the difference between the t and $\bar{t}$ rapidities, taking the forward direction to be that of the proton. The SM prediction for the inclusive asymmetry is

$$A_{\rm FB}^{\rm SM} = 0.088 \pm 0.006. \quad (40)$$

TABLE IV. Experimental input for $t\bar{t}$ production cross section and asymmetries. All errors have been added in quadrature.

Observable	Value	Reference
$A_{\mathrm{FB}}^{\mathrm{low,\,CDF}}$	0.084 ± 0.055	[46]
$A_{\mathrm{FB}}^{\mathrm{high,\,CDF}}$	0.295 ± 0.067	[46]
$A_{\mathrm{FB}}^{\mathrm{inc,\,CDF}}$	0.164 ± 0.047	[46]
$A_{\mathrm{FB}}^{\mathrm{inc,\,D0}}$	0.106 ± 0.030	[47]
$A_{\mathrm{FB}}^{\mathrm{inc,\,average}}$	0.124 ± 0.025	
$A_{\mathrm{C}}^{\mathrm{inc,\,ATLAS,\,semileptonic}}$	0.006 ± 0.010	[48]
$A_{\mathrm{C}}^{\mathrm{inc,\,ATLAS,\,dileptons}}$	0.057 ± 0.028	[49]
$A_{\mathrm{C}}^{\mathrm{inc,\,CMS,\,semileptonic}}$	0.004 ± 0.015	[50]
$A_{\mathrm{C}}^{\mathrm{inc,\,CMS,\,dileptons}}$	-0.010 ± 0.019	[51]
$A_{\mathrm{C}}^{\mathrm{inc,7\,TeV,\,average}}$	0.007 ± 0.008	
$A_{\mathrm{C}}^{\mathrm{inc,\,CMS,\,8\,TeV}}$	0.005 ± 0.009	[52]
$\sigma_{\mathrm{inc}}^{\mathrm{CDF+D0}}$	(7.60 ± 0.41) pb	[53]
$\sigma_{\mathrm{inc}}^{\mathrm{ATLAS}}$ (7 TeV)	(177 ± 11) pb	[54]
$\sigma_{\mathrm{inc}}^{\mathrm{ATLAS}}$ (8 TeV)	(237.7 ± 11.3) pb	[55]
$\sigma_{\mathrm{inc}}^{\mathrm{CMS}}$ (7 TeV)	(165.8 ± 13.3) pb	[56]
$\sigma_{\mathrm{inc}}^{\mathrm{CMS}}$ (8 TeV)	(239 ± 13) pb	[57]

This result uses NLO cross-section differences, including leading EW corrections, in the numerator [58,60–65] and LO cross sections in the denominator. Note that use of the NLO cross sections in the denominator would reduce the predicted asymmetry by $\mathcal{O}(30\%)$. The NLO Parton Distribution Functions (PDF) set CTEQ6.6M [66] is used throughout. The error in Eq. (40) is the pure scale uncertainty for $\mu \in [m_t/2, 2m_t]$.

The CDF [46] measurement of A_{FB} is larger than the SM prediction, as was the 2011 D0 measurement. A new D0 measurement [47], extended to include a 3-jet sample in $t\bar{t}$ production, is significantly lower and supersedes the previous one. Naively averaging with CDF yields

$$A_{\mathrm{FB}}^{\mathrm{inc}} = 0.124 \pm 0.025. \tag{41}$$

Interestingly, CDF observes a significant rise in A_{FB} with the invariant mass of the $t\bar{t}$ pair. Quoting just their two-bin result as an example, they report

TABLE V. SM predictions for $t\bar{t}$ production cross section and asymmetries.

Observable	Value	Reference
$A_{\mathrm{FB}}^{\mathrm{low,\,SM}}$	0.062 ± 0.003	[58]
$A_{\mathrm{FB}}^{\mathrm{high,\,SM}}$	0.129 ± 0.006	[58]
$A_{\mathrm{FB}}^{\mathrm{inc,\,SM}}$	0.088 ± 0.006	[58]
$A_{\mathrm{C}}^{\mathrm{SM}}$ (7 TeV)	0.0123 ± 0.0005	[58]
$A_{\mathrm{C}}^{\mathrm{SM}}$ (8 TeV)	0.0111 ± 0.0004	[58]
$\sigma_{\mathrm{inc}}^{\mathrm{TEV,\,NNLO}}$	(7.395 ± 0.544) pb	[59]
$\sigma_{\mathrm{inc}}^{\mathrm{LHC,\,NNLO}}$ (7 TeV)	(172.5 ± 15.0) pb	[59]
$\sigma_{\mathrm{inc}}^{\mathrm{LHC,\,NNLO}}$ (8 TeV)	$(246.3^{+19.8}_{-20.5})$ pb	[59]

$$A_{\mathrm{FB}}^{\mathrm{low}} = 0.084 \pm 0.046 \pm 0.030, \tag{42}$$

for $m_{t\bar{t}} \leq 450$ GeV and

$$A_{\mathrm{FB}}^{\mathrm{high}} = 0.295 \pm 0.058 \pm 0.033, \tag{43}$$

for $m_{t\bar{t}} \geq 450$ GeV, which should to be compared to the SM predictions [58]

$$A_{\mathrm{FB}}^{\mathrm{low,\,SM}} = 0.062 \pm 0.003 \tag{44}$$

and

$$A_{\mathrm{FB}}^{\mathrm{high,\,SM}} = 0.129 \pm 0.006. \tag{45}$$

The CDF and D0 collaborations have also presented results with finer, albeit different, binning in $m_{t\bar{t}}$ [46,47]. The two sets of measurements are consistent with each other, with the exception of the largest bin, $m_{t\bar{t}} > 650$ GeV, for which D0 obtains a negative central value with an error that is 68% larger than CDF's. In the $m_{t\bar{t}} \in [550, 650]$ bin, the D0 and CDF central values are very close, but the D0 error is 60% larger. The CDF fitted slope for A_{FB} vs $m_{t\bar{t}}$ is 1.8σ larger than D0's and 2.4σ larger than the NLO SM prediction. Both collaborations have also measured A_{FB} vs the rapidity difference Δy, again with different binning. The CDF fitted slope is 1.3σ larger than D0's and 2.4σ larger than the NLO SM prediction.

At the LHC, the initial state is symmetric, and thus there is no fixed forward or backward direction with respect to which an asymmetry can be defined. Instead, the observable that is related to A_{FB} is the charge asymmetry,

$$A_{\mathrm{C}} = \frac{N(\Delta|y| > 0) - N(\Delta|y| < 0)}{N(\Delta|y| > 0) + N(\Delta|y| < 0)}, \tag{46}$$

where $\Delta|y| = |y_t| - |y_{\bar{t}}|$ is the difference between the absolute values of the top and antitop rapidities. At 7 TeV both ATLAS and CMS have measured the charge asymmetry in the semileptonic and dilepton decay channels, albeit with appreciable experimental uncertainties (see Table IV). Naively averaging the four measurements yields

$$A_{\mathrm{C}}^{\mathrm{EXP}} = 0.007 \pm 0.008, \tag{47}$$

consistent with the SM prediction [58]

$$A_{\mathrm{C}}^{\mathrm{SM}} = 0.0123 \pm 0.0005. \tag{48}$$

(Only averaging the two semileptonic measurements yields $A_{\mathrm{C}}^{\mathrm{exp}} = 0.005 \pm 0.009$.) Again, the SM prediction has been obtained with the leading-order (LO) cross section in the denominator. An 8 TeV measurement of A_{C} was recently presented by CMS [52],

$$A_{\mathrm{C}} = 0.005 \pm 0.009, \tag{49}$$

which is also consistent with the SM prediction [58]

$$A_C = 0.0111 \pm 0.0004. \quad (50)$$

Whether or not the experimental situation at the Tevatron points to an anomalously large forward-backward asymmetry or is due to statistical fluctuations, our philosophy will be to show that in our model large enhancements of A_{FB} can be consistent with all other constraints, thus highlighting the stealth nature of the new strong interactions.

B. Choosing a benchmark

We calculate the asymmetries in our NP model using the procedure outlined in Ref. [33] and employed in Ref. [58] for the SM predictions given above. In the numerator we take the SM at NLO (QCD + EW) and work with LO cross sections in the denominators. The contributions from NP (including NP–SM interference) in both the numerator and denominator are always evaluated at LO. All LO cross sections are automatically evaluated in MADGRAPH [67] using the NLO PDF set CTEQ6M with a fixed renormalization and α_s scale. For the benchmark presented here, we fix the renormalization scale to $\mu = 2m_t$.

To obtain the Tevatron and LHC total $t\bar{t}$-production cross sections and differential $d\sigma/dm_{t\bar{t}}$ spectra, we use the next-to-next-to-leading-order (NNLO) CTEQ10 predictions [59] at $\mu = m_t$ for the total SM cross sections, with their reported errors (see Table V), and aMC@NLO for the differential SM spectra, evaluated at $\mu = m_t$, with the errors reflecting the scale and PDF uncertainties. The NP contributions to the total and differential spectra are evaluated at LO for a fixed scale choice, $\mu = 2m_t$, as in the asymmetries.

Two of the explanations that have been proposed for the potential Tevatron $A_{FB}^{t\bar{t}}$ anomalies are t-channel exchange of light vectors, e.g. W', Z' [30], or of light scalars [32]. In both cases the exchanged particle's mass is optimally a few hundred GeV or less. The models can yield a large $A_{FB}^{t\bar{t}}$ that, particularly in the case of vector exchange, increases appreciably with $m_{t\bar{t}}$. Moreover, both proposals have been shown to simultaneously lead to good agreement with the $d\sigma/dm_{t\bar{t}}$ spectra (for the t-channel exchanges, correcting for the CDF acceptance at large pseudorapidity is crucial [25,68,69]).

Our model provides a concrete renormalizable example that combines the two proposals. The role of the Z' is played by the HC K^* and, to a lesser extent, by the K_1. The t-channel scalar corresponds to the HC K. Note that for high $m_{t\bar{t}}$ there are also perturbative contributions coupling to the RH up-type quarks from intermediate $S - \mathcal{Q}$ box graphs, which scale as

$$\frac{h_1^2 h_3^2}{16\pi^2}\frac{1}{m_{t\bar{t}}^2} \sim \frac{1}{2m_{t\bar{t}}^2}. \quad (51)$$

However, we find that their effects are subleading and do not consider them further.

At the LHC important constraints come from $\sigma_{t\bar{t}}$ and A_C. An increase in $A_{FB}^{t\bar{t}}$ via t-channel exchange is typically correlated with an increase in A_C beyond its measured value. However, associated light-mediator production, e.g. $gq \to t + (Z' \to \bar{t}q)$ from Fig. 2, has been shown to reduce A_C [33]. Associated light-mediator production also contributes to the total LHC cross section, $\sigma_{t\bar{t}}$. The resulting constraint, as well as the ATLAS and CMS bounds from t + jet resonance searches, are evaded if the light mediator has other open decay channels, thus suppressing the $Z' \to \bar{t}q$ branching ratio. In our model a new dominant decay channel is naturally present. In particular, the strong interaction decay $K^* \to K\pi$ can lead to $\mathrm{Br}(K^* \to \bar{t}j) \sim \mathcal{O}(30\%)$. This would still allow for a significant reduction of A_C. Note that on-shell $K \to t + j$ decays are kinematically forbidden so that the above constraints do not apply.

Previous studies, as outlined above, thus motivate us to search for benchmarks with relatively light K^* and K, with masses of ~200 GeV. Moreover, a ρ mass in this range is also favored by the recent CDF bounds on pair production of dijets [70]. For $\rho \to \pi\pi \to jjjj$ with $m_\rho \lesssim 200$ GeV and $m_\pi \sim 70$ GeV, the bounds weaken significantly and, in fact, lie above the expected limits.

To obtain a viable set of parameters for our model that i) yields substantially enhanced $A_{FB}^{t\bar{t}}$ at the Tevatron and ii) yields agreement with all other constraints, we employ a rough χ^2-minimization procedure containing a subset of available measurements. Minimizing the χ^2 with respect to a large number of variables is algorithmically difficult. We use the COBYLA method [71], which allows us to apply constraints on the minimization procedure.

The χ^2 contains the experimental values of the inclusive $A_{FB}^{t\bar{t}}$ and A_C (7 TeV), the total $t\bar{t}$ cross sections at the Tevatron and the LHC (7 TeV), and the highest bins of the differential cross sections at ATLAS (7 TeV) and CMS (8 TeV). The UV inputs are $h_1, h_3, m_{\mathcal{Q}_1}, m_{\mathcal{Q}_3}, m_S$, and the HC scale M_χ defined in Eq. (17). Through dimensional transmutation, the latter is equivalent to the choice of HC strong coupling constant, α_{HC}, in the UV. The UV parameters fix the pseudoscalar masses via the quadratic terms in the HC chiral Lagrangian and the vector and axial-vector masses via the naive quark model described in

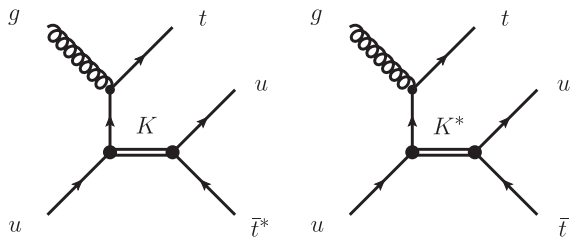

FIG. 2. Feynman diagrams for the associated production of a K and K^*, respectively. The $\bar{t}$ resulting from the K decay is off shell.

Appendix A. The would-be composite quark masses in the interaction basis are given by Eq. (A17). The decay constants f_π, f_ρ, and f_{a_1} (for simplicity taken to be universal for all members of the corresponding flavor octets), are given in Eqs. (18)–(20). The would-be composite quark decay constants $f_{u_i'}$ are allowed to vary within 30% of the interpolation given in Eq. (B5).

We must also choose values for the couplings of the HC resonances to the would-be composite quarks, i.e. g_ρ, g_{a_1}, and g_A. We allow g_ρ and g_{a_1} to lie within roughly 30% of the values obtained from Eq. (32), and we take $g_A = 1.26$, identifying it with the representative QCD nucleon-pion axial coupling. The vector-pion coupling $g_{\rho\pi\pi}$ is taken to be equal to g_ρ. The decay widths of the vector-meson multiplet, $\rho, K^*, \ldots$, are determined via Eqs. (C1)–(C3). The axial decay widths are determined using the model of Ref. [42], see Eqs. (C8)–(C12), with the parameter $\tilde{F}_{\rm HC}$ fixed to the value obtained from Eq. (C12). The pseudoscalar decay widths (38) are small and do not enter into our analysis.

The UV or fundamental parameters for our illustrative benchmark are listed in Table II, together with the resonance couplings and decay constants. The resonance masses and decay widths are given in Table I. Realization of the phenomenologically favored range $\mathrm{Br}(K^* \to \bar{t}j) \sim 30\%$ arises via phase-space suppression of the dominant $K^* \to K\pi$ decay mode; see Table III. Since $m_K^* \simeq m_K + m_\pi$ the phase-space factor is small, of $O(10^{-2})$ in our benchmark. The tuning associated with the phase-space suppression is actually quite moderate, given that the approximate equality of m_K^* and $m_K + m_\pi$ changes relatively slowly as the HC quark masses $m_{\mathcal{Q}_3}$, $m_{\mathcal{Q}_1}$ are varied. For instance, the Barbieri–Giudice measure of fine-tuning for the phase-space suppression factor, corresponding to variation of the HC quark masses around the benchmark point and using the naive quark model for the vector masses, is ≈8. It is comparable to the tuning associated with the coincidence of m_ϕ and $2m_K$ in QCD.

Before moving to the resulting phenomenology, we comment on the large benchmark Yukawa couplings $h_3 = 4.2$, $h_1 = 2.0$. This is driven by two factors: a sizable product of couplings $h_1 h_3$ is required in order to obtain a large t-channel enhancement of the forward-backward asymmetry, e.g. $A_{\rm FB} > 0.15$, and h_1 is bounded from above by dijet constraints, most notably the CDF bounds on dijet pair production; see below. A moderate decrease in h_3 is possible if the nonperturbative couplings g_ρ or g_A of the vector or pseudoscalar mesons to the would-be composite quarks are moderately increased, or if h_1 is maximized consistently with dijet phenomenology. Nevertheless, a large h_3 is required, e.g. $h_3 > 3$.

The values of the Yukawa couplings h_1, h_3 in Table II correspond to a renormalization scale which can be approximately identified with $m_{\mathcal{S}}$. A large h_3 at this scale prompts us to ask if our theory is sensible at higher energies. For example, whether we encounter a Landau pole as we evolve h_1, h_3, and the HC gauge coupling $g_{\rm HC}$ upward in energy. To answer this, we fix the values of $h_1(m_{\mathcal{S}})$, $h_3(m_{\mathcal{S}})$ to those given in Table II. We also take $g_{\rm HC}(m_{\mathcal{S}}) = 1.9$, the value we would obtain for the QCD coupling g_s at scale $\mu = m_{\mathcal{S}} f_\pi / f_\pi^{\rm HC}$ by running upward with three flavors rather than four (given the three HC quark flavors) from its usual two-loop $\overline{\rm MS}$ value at $\mu = 1$ GeV. The one-loop RGEs yield a Landau pole at $\mu \approx 1.6$ TeV. However, moving to two-loop RGEs using the general results from Ref. [72], we find that h_3 reaches an approximate attractive UV fixed point at $\mu = O(10)$ TeV, given by $h_3^* = 16\pi/\sqrt{37} \approx 8.3$, while h_1 and $g_{\rm TC}$ are asymptotically free. For lower values of $h_3(m_{\mathcal{S}}) > 3$ (see above), with $h_3(m_{\mathcal{S}}) > h_1(m_{\mathcal{S}})$, the one-loop Landau pole and the two-loop UV fixed point for h_3 are, respectively, reached at scales that are a few times larger. Clearly, given the large value of h_3^* obtained at two loops, the question of whether a true UV fixed point exists or not can only be settled using nonperturbative methods.

Consistency of our model requires that there are no QCD and HC breaking condensates, $\langle \bar{u}_{R3} \mathcal{Q}_{L3} \rangle \neq 0$ and $\langle \mathcal{S} \rangle \neq 0$, which could potentially be triggered by a large value of h_3. An estimate of the critical Yukawa coupling above which condensates form can be obtained using the Schwinger–Dyson equation at one-loop in the rainbow or ladder approximation in the massless scalar limit (see Ref. [73], where such an estimate was applied to electroweak-symmetry breaking via fourth-family condensates with large Higgs Yukawa couplings). In our model, the ladder approximation in the $m_{\mathcal{S}} = 0$ limit yields $h_3^{\rm crit} = 2\pi$, somewhat below the two-loop fixed point coupling h_3^*. If this result also holds nonperturbatively, the field content of the theory would need to be enlarged in order for the model to be phenomenologically viable. For example, we have checked that the addition of massive singlets, $\mathcal{N}_i$, with flavor conserving Yukawa couplings to the HC quarks,

$$h^i_{\mathcal{N}1} \mathcal{N}_i (\bar{\mathcal{Q}}_1 \mathcal{Q}_1 + \bar{\mathcal{Q}}_2 \mathcal{Q}_2) + h^i_{\mathcal{N}3} \mathcal{N}_i \bar{\mathcal{Q}}_3 \mathcal{Q}_3, \tag{52}$$

lead to an asymptotically free h_3, with h_3 always well below 2π, for a large set of $h^i_{\mathcal{N}1,2}$ values. In this case some or all of the singlet Yukawas, $h^i_{\mathcal{N}1,2}$, obtain a fixed point. The presence of the singlets also has an added benefit that the HC quark masses, $m_{\mathcal{Q}}$, can be generated dynamically via the induced singlet vevs.

C. Top-antitop asymmetries and cross sections: Benchmark predictions

The predictions for the Tevatron $t\bar{t}$ asymmetries within our benchmark are (quoting the central values)

$$A_{\rm FB}^{\rm inc} = 0.173, \qquad A_{\rm FB}^{\rm low} = 0.091, \qquad A_{\rm FB}^{\rm high} = 0.301, \tag{53}$$

corresponding to a large enhancement of $A_{\rm FB}$ at large $m_{t\bar{t}}$. On the other hand, the charge asymmetries at the LHC are predicted to be

$$A_{\rm C}^{\rm inc,\,7\,TeV} = 0.0137, \qquad A_{\rm C}^{\rm inc,8\,TeV} = 0.0135, \tag{54}$$

consistent with the SM predictions, as well as their measured values. Note that the associated production of K^* has a significant effect on the value of $A_{\rm C}$. Without this effect the charge asymmetries would have been $A_{\rm C}^{\rm inc,\,7\,TeV} = 0.0245$, and $A_{\rm C}^{\rm inc,\,8\,TeV} = 0.0239$. The total cross sections at the Tevatron and the LHC are found to be

$$\begin{aligned} \sigma_{\rm inc}^{\rm TEV} &= 6.34 \pm 0.54 \text{ pb}, \\ \sigma_{\rm inc}^{\rm LHC}(7 \text{ TeV}) &= 176 \pm 15 \text{ pb}, \\ \sigma_{\rm inc}^{\rm LHC}(8 \text{ TeV}) &= 252 \pm 20 \text{ pb}, \end{aligned} \tag{55}$$

where the errors reflect the uncertainty in the SM contributions at NNLO, as discussed above. These predictions are in good agreement with the experimental measurements, listed in Table IV, with the exception of a $\sim 2\sigma$ tension with the larger measured value of $\sigma_{\rm inc}^{\rm TEV}$. Note that the NP contributions to all observables have been treated at leading order and are therefore subject to significant uncertainties which have not been included in our predictions.

The differential forward-backward asymmetries $dA_{\rm FB}/dm_{t\bar{t}}$ and $dA_{\rm FB}/d|\Delta y|$ are compared to the CDF data[3] and the SM predictions in Fig. 3. The CDF differential cross section is shown in Fig. 4 (left). The dominant NP effect on $t\bar{t}$ production in our model is due to t-channel exchanges. Thus, the effect of the CDF rapidity acceptance corrections for large $m_{t\bar{t}}$ is significant [68,69]. We take this into account using the prescription in Ref. [25]. In Fig. 4 we compare the predicted normalized differential cross section, $1/\sigma d\sigma/dm_{t\bar{t}}$, with the 7 TeV ATLAS [74] and 8 TeV CMS [75] measurements for semileptonic final states. We can see that it is not difficult to reproduce the increase in $A_{\rm FB}$ vs $m_{t\bar{t}}$ and $A_{\rm FB}$ vs Δy. A modest indication of the well-known high $m_{t\bar{t}}$ tail in the LHC $d\sigma/dm_{t\bar{t}}$ distribution, characteristic of low-scale t-channel exchanges [30,76], can be seen in the last bin of the second as well as the third panels of Fig. 4. It lies well within the experimental uncertainties.

The deficit in the inclusive $t\bar{t}$ cross section at the Tevatron, $\sigma_{\rm inc}^{\rm TEV}$, is primarily due to the lowest bin, as can be seen in Fig. 4 (first panel). Note that a relative increase in the scalar (K) vs vector (K^*, K_1) contributions to $t\bar{t}$ production would reduce this deficit. This could be achieved by increasing the coupling g_A relative to g_{ρ,a_1}.

[3]Since our main point is to provide an explicit model which can explain a large asymmetry while being consistent with all other data, we compare our predictions to the CDF measurements, which yield larger slopes than D0's.

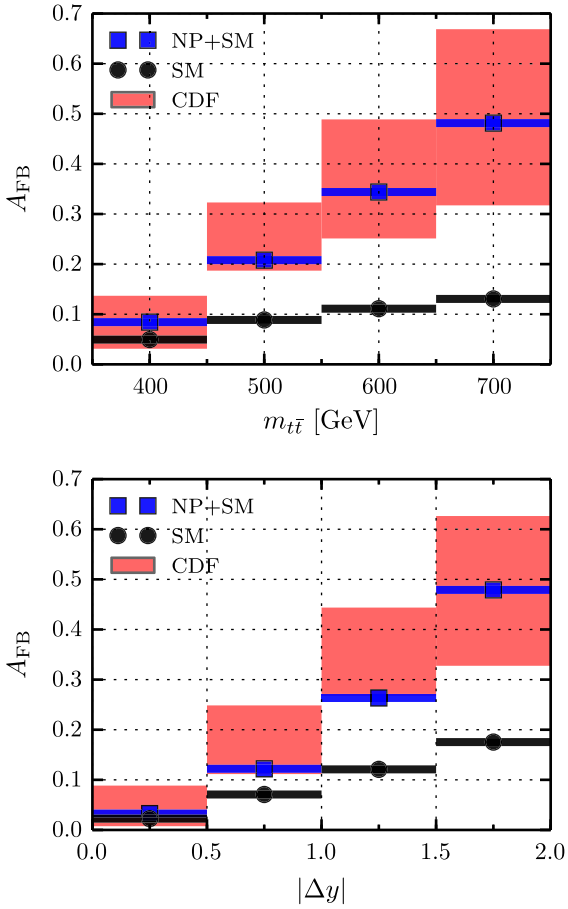

FIG. 3 (color online). Differential $A_{\rm FB}$ asymmetries at the Tevatron as a function of $m_{t\bar{t}}$ (top) and Δy (bottom) with the SM prediction in black, the NP benchmark predictions in blue, and the measurements by CDF given by red bands.

D. Dijets

The dijet cross-section measurements at the Tevatron and the LHC typically provide stringent constraints on models that aim to explain the forward-backward asymmetry in $t\bar{t}$, since the resonances are usually required to have large couplings to quarks. The s-channel exchanges are subject to direct resonance searches (i.e. bump hunting in $pp \to 2j$), while t-channel exchanges could visibly enhance the $d\sigma_{jj}/dm_{jj}$ spectra at large invariant masses [25].

The couplings of the various resonances to light-quark pairs in our benchmark are summarized in Table VI. Dijet production in the s channel is primarily due to ρ, ω, and a_1 exchanges. The ρ, ω, and a_1 contributions are suppressed by their relatively small couplings to light quarks. This is a result of the hierarchy between h_1 and h_3; see Table II. Moreover, the ρ and a_1 contributions are further suppressed by their small branching ratios to quark pairs (they predominantly decay to pseudoscalar–pseudoscalar and vector–pseudoscalar pairs, respectively; cf. Tables III, VII, and VIII for the branching ratios of the subsequent pseudoscalar decays). Finally, the s-channel contributions

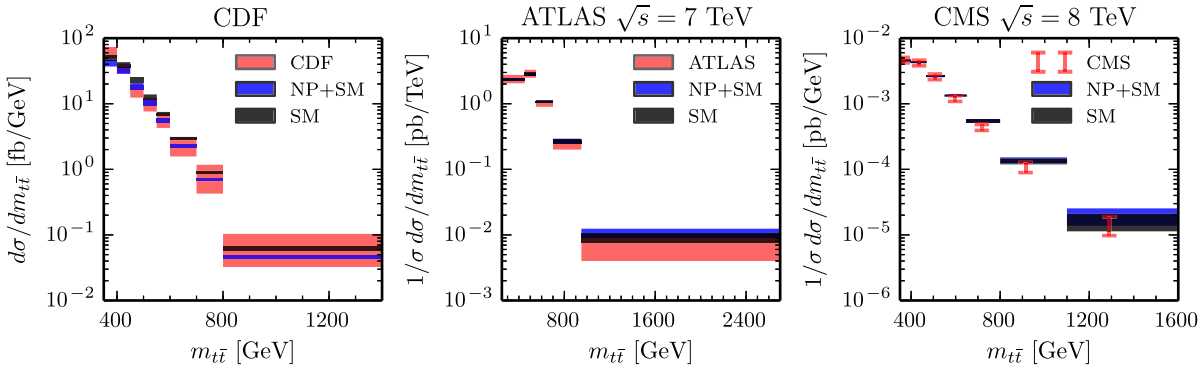

FIG. 4 (color online). The differential cross sections, $d\sigma/dm_{t\bar{t}}$, at the Tevatron (first panel) and at the LHC (7 TeV ATLAS in the second panel and 8 TeV CMS in the third panel), SM prediction in black, the NP benchmark predictions in blue, and measurements by CDF given by red bands.

of the pseudoscalars are negligible because of the chiral suppression of their couplings to light quarks.

All of the above resonances also contribute in the t-channel. Here, the branching ratios to dijets play no role, since the resonance contributions only depend on their couplings to the light quarks. The modest hierarchy $h_1 < h_3$ in Eq. (4) turns out to be crucial. For instance, had we taken $h_1 \simeq h_3$, the t-channel exchanges would yield an appreciable $\mathcal{O}(1)$ excess at $m_{jj} = 3$ TeV.

In Figs. 5 and 6, we compare the benchmark and SM $d\sigma_{jj}/dm_{jj}$ dijet mass spectra at the Tevatron and LHC (8 TeV). The dijet cross sections are calculated at the partonic level at LO, using MADGRAPH with CTEQ6M and NLO α_s. Guided by the experimental analyses [77,78], we impose the following cuts on the two outgoing partons (i.e. the two leading jets). For the Tevatron we impose $|y| < 1$. For the 8-TeV LHC cross section calculation, we require that the pseudorapidity difference between the two partons satisfies $\Delta\eta_{jj} < 1.3$ and that $|\eta| < 2.5$, $p_T > 30$ GeV for each of them. The renormalization scale is set to the average p_T of the outgoing partons in both cases. In the LHC analysis, the dijet mass is above $m_{jj} > 890$ GeV.

The upper two panels in Figs. 5 and 6 show $d\sigma_{jj}/dm_{jj}$ in the SM (black line) and in our benchmark (red line). The lower two panels show the ratios of the two, $(d\sigma_{jj}^{\rm NP}/dm_{jj})/(d\sigma_{jj}^{\rm SM}/dm_{jj})$. The effect of the new resonance exchanges is small, lying below the experimental uncertainties at both the Tevatron and the LHC. In both cases the experimental analysis was aimed at bounding resonance production in the dijet channel. The CDF bump-hunting analysis allows for about a 1%–2% spread in the ratio of data to a smooth background for $m_{jj} \in [200, 700]$ GeV. This spread is larger than the deviation of $(d\sigma_{jj}^{\rm NP}/dm_{jj})/(d\sigma_{jj}^{\rm SM}/dm_{jj})$ from 1, as shown in the lower panel of Fig. 5. Furthermore, our benchmark does not show any bumps in the spectrum at this level of precision. The CMS bump-hunting analysis allows for a NP contribution in the m_{jj} spectrum at the level of a few per

TABLE VI. Table of the dominant branching ratios of HC pions into SM quarks.

HC resonance	Channel	Br(%)
$\pi_{\rm HC}$	$\bar{u}c, \bar{c}u, \bar{u}u + \bar{c}c$	100
$K_{\rm HC}$	$\bar{u}t, \bar{t}u, \bar{c}t, \bar{t}c$	100
$\eta_{\rm HC}$	$\bar{u}u + \bar{c}c$	100

TABLE VII. Table of the dominant branching ratios for HC axial-vector resonances and their decays to the SM quarks.

HC resonance	Channel	Br(%)
a_1	$\rho\pi$	99.08
	$\bar{u}c, \bar{c}u, \bar{u}u + \bar{c}c$	0.92
K_1	ρK	92.6
	$\bar{u}t, \bar{t}u, \bar{c}t, \bar{t}c$	7.4
A_L	$\bar{u}u + \bar{c}c$	100
A_H	$\bar{u}u + \bar{c}c$	100

TABLE VIII. HC resonance couplings to SM quarks. They correspond to the coefficients in the Lagrangian of Eq. (33) after rotating all fields to the mass eigenbasis.

HC resonance	Quarks	κ_R^V	κ_L^V
ρ	$\bar{u}u, \bar{c}c$	± 0.117	0.0
	$\bar{u}c$	0.165	0.0
K^*	$\bar{u}t, \bar{c}t$	0.328	0.0
V_L	$\bar{u}u, \bar{c}c$	0.117	0.0
	$\bar{t}t$	−0.018	−0.001
V_H	$\bar{u}u, \bar{c}c$	−0.003	0.0
	$\bar{t}t$	−0.649	−0.038
a_1	$\bar{u}u, \bar{c}c$	± 0.161	0.0
	$\bar{u}c$	0.228	0.0
K_1	$\bar{u}t, \bar{c}t$	0.451	0.0
f_1	$\bar{u}u, \bar{c}c$	0.160	0.0
	$\bar{t}t$	−0.116	−0.007
f_1'	$\bar{u}u, \bar{c}c$	−0.021	0.0
	$\bar{t}t$	−0.887	−0.052

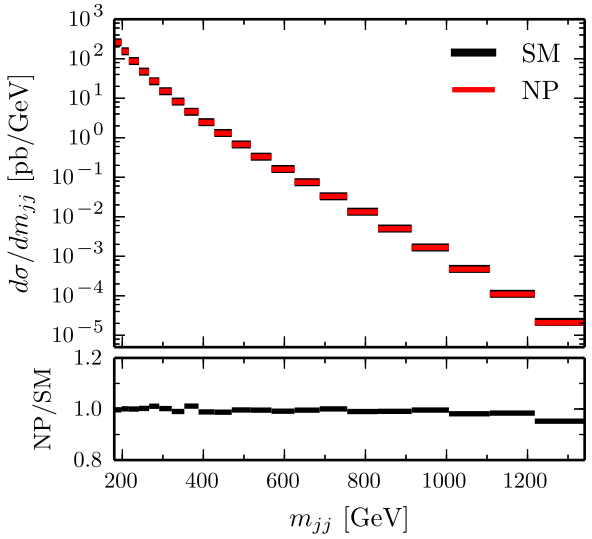

FIG. 5 (color online). The dijet cross-section distribution at CDF.

mill at $m_{jj} \sim 1000$ GeV, with an increase to $\mathcal{O}(10\%)$ at $m_{jj} \sim 3000$ GeV. Note that the benchmarks differential distribution is very smooth. Fitting $d\sigma_{jj}^{\rm NP}/dm_{jj}$ to the same analytical function that was used to describe the smooth QCD background in Ref. [78], we find that the difference between the fit and the prediction is always well below a per mill. Thus, the bump-hunting analysis is not sensitive to our model.

CMS and D0 have also measured the dijet angular distributions $d\sigma/d\chi$ as functions of the dijet mass [here, $\chi = \exp(|y_1 - y_2|)$, where y_1 and y_2 are the rapidities of the two leading jets] [79,80]. The comparison of our benchmark and SM predictions are shown in Fig. 7 for the Tevatron and in Fig. 8 for the LHC. The predictions are

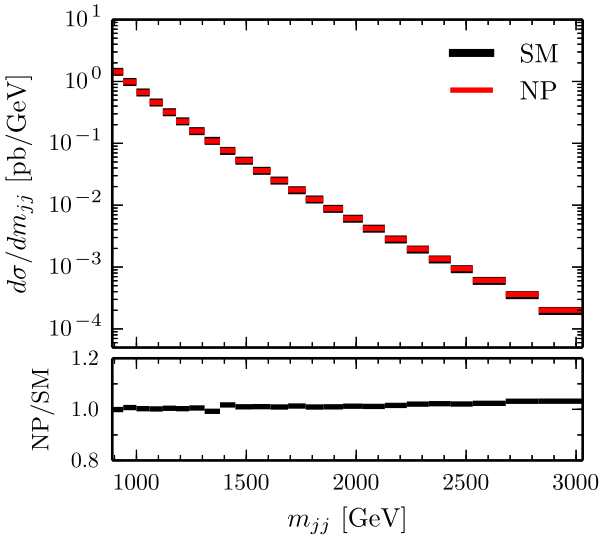

FIG. 6 (color online). The dijet cross-section distribution at CMS.

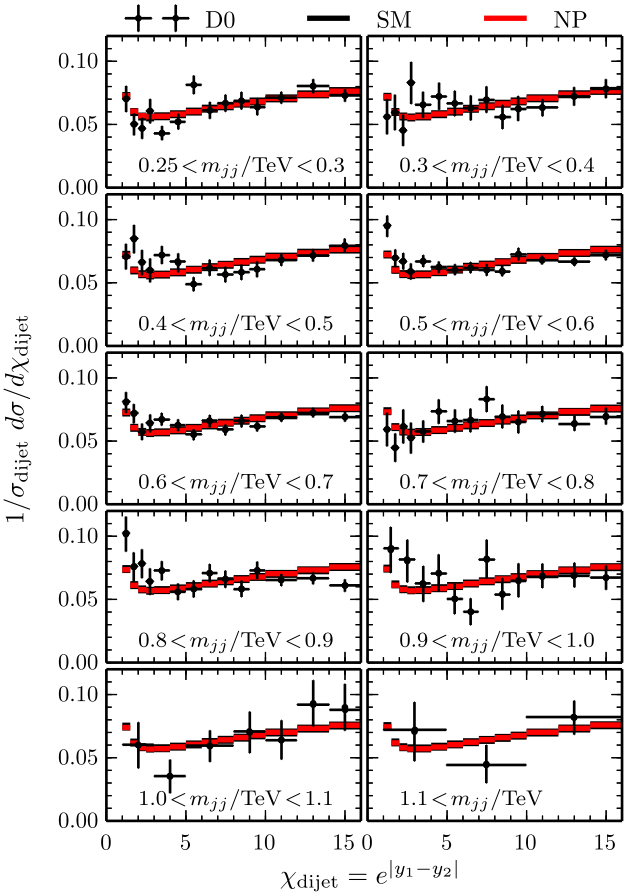

FIG. 7 (color online). The dijet angular distributions at the Tevatron, in bins of m_{jj}. The SM predictions are denoted by black lines, the benchmark predictions are in red, while measurements are denoted with crosses of the size of error bars.

calculated at LO at the partonic level using MADGRAPH with CTEQ6M PDFs, setting the renormalization scale to the average p_T of the outgoing partons. Following the D0 analysis, we impose the Tevatron cut $y_{\rm boost} \equiv 0.5|y_1 + y_2| < 1$, where $y_{1,2}$ are now the rapidities of the two partons (as opposed to the rapidities of the two leading jets). The D0 measurements begin at $m_{jj} > 250$ GeV. Following the CMS angular analysis, we impose the LHC cut $y_{\rm boost} < 1.11$. The CMS measurements begin at $m_{jj} > 400$ GeV. The contributions from the NP resonances lead to deviations from the SM predictions that are much smaller than the experimental error bars. In the figures we show the LO predictions for the SM; however, the NLO predictions are available [81,82]. They further improve the agreement between the data and the SM predictions. Our conclusion that the NP contributions to the angular distributions are negligible is not expected to change when going from LO to NLO predictions.

Another constraint arises from searches for pair production of resonances that decay to dijets, resulting in 4-jet final states. In our model this signal would be due to s-channel ρ production followed by $\rho \to \pi\pi$ decays with $\pi \to jj$.

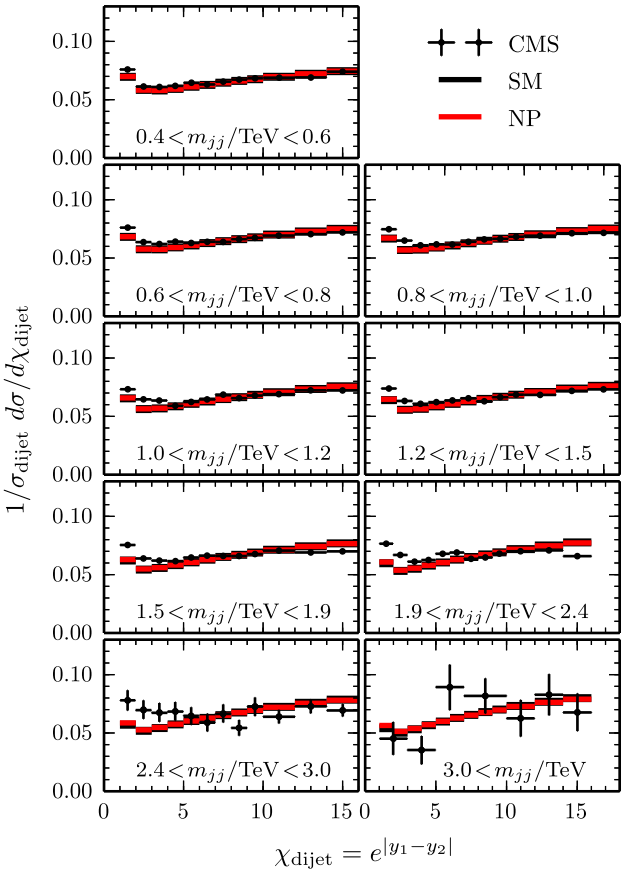

FIG. 8 (color online). The angular distributions in dijet production at the LHC, measured in bins of m_{jj} as indicated in the plots. The SM prediction is denoted by black lines, the prediction with our benchmark NP is in red, while crosses denote the measured spectra including errors.

The 95% C.L. bound on $\sigma(p\bar{p} \to X \to YY \to jjjj)$ from CDF for $m_X = 175$ GeV and $m_Y = 50(70)$ GeV is 66.8 (111.5) pb [70]. In our benchmark, $X = \rho$ with a mass of 177 GeV, and $Y = \pi$ with a mass of 62 GeV. The inclusive production cross section at LO is ≈79 pb. However, after imposing partonic cuts based on the CDF hadronic jet cuts ($p_T^{\text{min}} > 15$ GeV and $|\eta| < 2.4$), we obtain $\sigma(p\bar{p} \to \rho \to \pi\pi \to jjjj) = 37$ pb. The $O(\alpha_s)$ Z' production K-factor, $1 + 8\pi\alpha_s(\mu)/9$, increases this cross section by ≈30% (at $\mu = m_\rho = 177$ GeV) to 48 pb. The analyses of pair production of dijets at CMS and ATLAS probe $m_{jj} > 250$ GeV and $m_{jj} > 150$ GeV [83,84], respectively, and are thus not sensitive to the $pp \to \rho \to \pi\pi$ mode in our model. However, they could be relevant for production of higher resonances, which we cover in the next section.

E. Production of new states

In this section we discuss existing constraints on the production of HC resonances in our model. As already mentioned, the CDF [85], CMS [86], and ATLAS [87] collaborations have searched for $t + j$ resonances, which could, in principle, constrain associated $K^* t$ and $K_1 t$ production. The CDF and ATLAS analyses put bounds on $t + j$ resonance masses above $m_{tj} > 200$ GeV and are thus relevant for our model (the CMS obtains bounds for $m_{tj} > 400$ GeV). The associated $K^* t$ and $K_1 t$ cross sections are listed in Table IX. Here, we sum over the *CP* conjugate final states $K^* t$ and $\bar{K}^* \bar{t}$ as well as over the light flavors, $K_{13}^* \sim [Q_1 \bar{Q}_3]$ and $K_{23}^* \sim [Q_2 \bar{Q}_3]$, and similarly for the K_1. At the 7 TeV LHC, one has $\sigma_{K^* t} Br_{K^* \to \bar{t} j} = 4.4$ pb, which is roughly a factor of 5 below the ATLAS bound for $m_{K^*} = 211$ GeV [87]. At the Tevatron, $\sigma_{K^* t} Br_{K^* \to \bar{t} j} = 0.07$ pb, which is roughly an order of magnitude smaller than the CDF bound [85]. In the case of associated K_1 production, the products $\sigma_{K_1 t} Br_{K_1 \to \bar{t} j}$ lie even further below the corresponding bounds at the Tevatron and the LHC.

Associated Kt production leads to a $\bar{t}^* t j$ final state, with one of the top quarks off shell. This feeds into the experimental measurements of the (inclusive) $t\bar{t}$ cross sections [55,57,88] and the Wt production cross section [89,90]. The Kt cross section is comparable to the theory error on the SM prediction for $t\bar{t}$ production. Furthermore, since the t^* is off shell, only a fraction of the Kt signal spills over into the $t\bar{t}$ production cross-section measurements. For instance, using a LO MADGRAPH analysis and imposing the experimental cuts for the $t\bar{t}$ signal region employed in the recent CMS dileptonic analysis [57], we estimate the Kt contribution to the 8 TeV $t\bar{t}$ cross section to be below 11 pb. It is thus smaller than the error on the measurement $\sigma(pp \to t\bar{t}) = 239 \pm 13$ pb [57]. The softer Kt lepton p_T significantly reduces the leakage into the signal region. Similarly, the Kt contribution to the Wt production signal region in the recent CMS dilepton analysis at 7 TeV is below 1.7 pb, to be compared with the CMS measurement of $\sigma(pp \to Wt) = 16^{+5}_{-4}$ pb [89].

Next we move to pair production of the colored scalars, $\mathcal{S}\mathcal{S}^*$. As discussed in Sec. III C, the decay width of the $\mathcal{S}$ is almost an order of magnitude greater than the HC hadronization scale $\Lambda_{\text{HC}} \sim \mathcal{O}(\text{few}) f_\pi$. Therefore, the $\mathcal{S}$ scalars decay before they can hadronize. This is reminiscent of the top quark in QCD. The $\mathcal{S}$ decays to quark–HC-quark pairs, $\mathcal{S} \to u_i \bar{\mathcal{Q}}_i$, where $i = 1, 2, 3$. The $\bar{\mathcal{Q}}_i$ from $\mathcal{S} \to u_i \bar{\mathcal{Q}}_i$ and the $\mathcal{Q}_j$ from $\mathcal{S}^* \to u_j \bar{\mathcal{Q}}_j$ hadronize via HC strong interactions and result in final states containing many π_{HC}, K_{HC}. In general we expect $pp \to \mathcal{S}\mathcal{S}^* \to u_i \bar{u}_j X_{\bar{\mathcal{Q}}_i \mathcal{Q}_j}$, where $X_{\bar{\mathcal{Q}}_i \mathcal{Q}_j}$ is the multi-π, K state. The light π will receive sizable boosts.

TABLE IX. Inclusive cross sections for $pp \to K_{\text{HC}}^{(*)} t$ and $pp \to K_1^{(*)} t$ associated production at the Tevatron and LHC 7 TeV, 8 TeV, and 13 TeV (in pb). Summation over the first two generations $\mathcal{Q}_{1,2}$ and the *CP*-conjugate modes is assumed.

Final state	σ_{TEV}	σ_{LHC7}	σ_{LHC8}	σ_{LHC13}
Kt	0.38	18.0	24.2	64.5
$K^* t$	0.22	13.6	18.5	50.6
$K_1 t$	0.11	11.1	15.4	45.1

TABLE X. Cross sections for LHC pair production of the HC scalars $\mathcal{S}\,\mathcal{S}^*$, at various center-of-mass energies.

$\sqrt{s}$	7 TeV	8 TeV	13 TeV
σ (pb)	1.62	2.76	13.17

Thus, a $\pi \to jj$ decay will on average appear as a single "fat jet" in the detector. However, fat jets from the heavier $K \to t^* + j$ decays should be easier to resolve.

The $\mathcal{S}\mathcal{S}^*$ production cross section at the 8 TeV LHC is 2.76 pb in the narrow-width approximation (cf. Table X). Taking into account the large $\mathcal{S}$ decay width ($\Gamma_{\mathcal{S}} \approx 0.44 M_{\mathcal{S}}$), we find that the $pp \to \mathcal{S}\mathcal{S}^* \to u_i \bar{u}_j X_{\bar{\mathcal{Q}}_i \mathcal{Q}_j}$ cross section is reduced to 1.4 pb in MadGraph. The dominant contributions are $pp \to \mathcal{S}\mathcal{S}^* \to q_{1,2}\bar{t} X_{\bar{\mathcal{Q}}_{1,2}\mathcal{Q}_3}$ and the CP conjugate modes, with a total cross section of 0.66 pb, and $pp \to \mathcal{S}\mathcal{S}^* \to t\bar{t} X_{\bar{\mathcal{Q}}_3 \mathcal{Q}_3}$, with a cross section of 0.57 pb. In Fig. 9 we show the mass distributions for $pp \to \mathcal{S}\mathcal{S}^* \to q_{1,2}\bar{t} X_{\bar{\mathcal{Q}}_{1,2}\mathcal{Q}_3}$; the distributions for the other decay modes of the $\mathcal{S}$ are very similar. One can see that the bulk of the $X_{\bar{\mathcal{Q}}_{1,2}\mathcal{Q}_3}$ system has invariant masses that lie above $\Lambda_\chi \sim \mathcal{O}(250)$ GeV and also well above the threshold for multipion production. There is enough energy available to produce tjK, $tjK + \pi$, $tjK + 2\pi$, etc., multipion final states. The cross section for producing one, two, three, or more HC pions depends on the details of the HC dynamics, and thus on the hadronization model. One could contemplate rescaling the hadronization models used for QCD to the HC scale to obtain a more quantitative description. However, for our purposes a qualitative picture suffices.

If we were to model the hadronization of the $\bar{\mathcal{Q}}_{1,2}\mathcal{Q}_3$ pair with a string model, the extra pions would be created from string breaking. Since there is sufficient energy, the penalty for creating an extra pion is small. As we saw, pair production of $\mathcal{S}\mathcal{S}^*$ would result in $tj + n$ fat jets (the HC pions and kaons) or $t\bar{t} + n$ fat jets final states. Here, n can lie anywhere from 1 to $\mathcal{O}(10)$. The $\mathcal{S}\mathcal{S}^*$ pair can thus be searched for in multijet final states. Both the CMS and ATLAS collaborations have recently made significant progress in multijet searches [91–93]. Particularly relevant in this respect is the ATLAS search [93], which was interpreted in terms of gluino production with R-parity violating decays that result in either 6-jet or 10-jet final states (in the 6-jet search, an extra initial-state radiation jet was required in order to optimize the sensitivity). Most importantly, the search strategy did not require the jets to form resonances of a particular mass and can thus be used to place bounds on the production of wide resonances, such as $\mathcal{S}\mathcal{S}^*$. For a 520 GeV gluino that decays to tjj, the ATLAS bound is $\sigma(pp \to \tilde{g}\tilde{g} \to \bar{t}t + 4j) < 0.9$ pb. This bound lies above the cross section for $\sigma(pp \to \mathcal{S}\mathcal{S}^* \to t\bar{t} + n\pi)$ in our model.

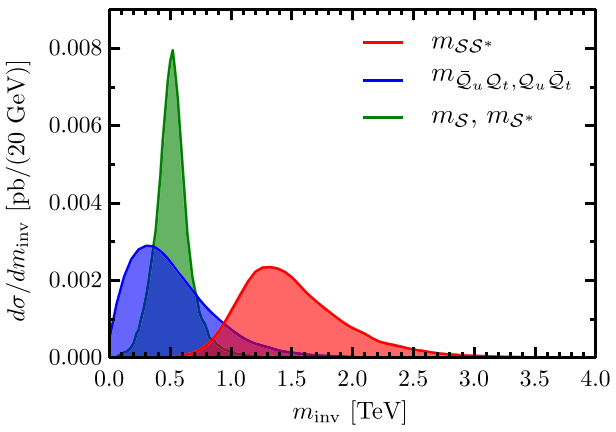

FIG. 9 (color online). The invariant mass distributions for $pp \to \mathcal{S}\mathcal{S}^* \to q_{1,2}\bar{t} X_{\bar{\mathcal{Q}}_{1,2}\mathcal{Q}_3}$. The $\mathcal{S}\mathcal{S}^*$ pair invariant masses are in red, the $X_{\bar{\mathcal{Q}}_{1,2}\mathcal{Q}_3}$ HC multipion invariant masses are in blue, and the individual invariant mass distributions of the $\mathcal{S}$ and $\mathcal{S}^*$ are similar and shown in green.

The ATLAS collaboration has also performed a search in which the final state contains $t\bar{t} + 2b$ jets and a number of light jets. This final state arises in our model from $pp \to \mathcal{S}\mathcal{S}^* \to t\bar{t}K\bar{K}$ plus any number of other pNGBs (a much smaller contribution could come from the ϕ resonance in place of $K\bar{K}$). Here, the hadronization of HC quarks results in a $K\bar{K}$ pair. The kaons then decay to off-shell t^* so that $K \to t^* j \to b3j$. We thus have $pp \to \mathcal{S}\mathcal{S}^* \to t\bar{t}2b6j$. The ATLAS search [93], with a gluino decaying to five quarks through an intermediate neutralino, gives an upper bound of about 1.5 pb, well above our production cross section of 0.6 pb.

V. ELECTROWEAK PRECISION TESTS, HIGGS COUPLINGS

In this section we discuss the implications of electroweak-precision measurements for our model. For the contributions to the electroweak oblique parameters S and T due to new HC states, we rely on the operator product expansion and quark hadron duality in order to estimate these contributions. Thus, the electroweak corrections are given by the diagrams in Fig. 10 to good approximation. The corrections are suppressed by powers of $\Lambda_{\rm HC}/m_{\mathcal{S}}$. The scalar $\mathcal{S}$ is an SU(2) singlet and thus does not contribute to the S parameter. The contribution to the T parameter, on the other hand, vanishes due to a cancellation between the two diagrams shown in Fig. 10 (see also the discussion of models with Higgs singlets in Ref. [94]). The HC quarks are hypercharge singlets and thus do not contribute at this order.

In Ref. [95] atomic-parity violation was advocated as a strong constraint on t-channel explanations of the forward-backward asymmetry.[4]

[4]Note that in the case of the general vector boson discussion the results of Ref. [95] [in Eq. (7)] are only indicative of the full UV result, as signaled by the gauge-parameter dependence of the displayed finite terms.

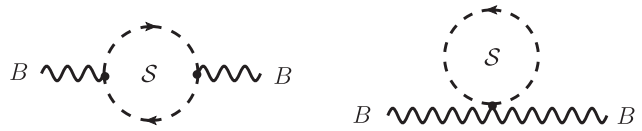

FIG. 10. The two contributions of the scalar $\mathcal{S}$ to the T parameter cancel.

Below the electroweak scale atomic-parity violation can be described by an effective electron-quark interaction of the form

$$\mathcal{L} = \frac{G_F}{\sqrt{2}} \sum_{q=u,d} (C_{1q} \bar{e}\gamma^\mu \gamma_5 e \bar{q}\gamma_\mu q + C_{2q} \bar{e}\gamma^\mu e \bar{q}\gamma_\mu \gamma_5 q), \quad (56)$$

where the second term is suppressed by the small electron weak charge and neglected in the following. We define the coupling between the Z boson and light quarks as in Ref. [95] by

$$\mathcal{L} = -\frac{e}{s_w c_w} Z^\mu (a_R^{\rm NP}(q) \bar{q}_R \gamma_\mu q_R + a_L^{\rm NP}(q) \bar{q}_L \gamma_\mu q_L). \quad (57)$$

In terms of the effective electron-quark Wilson coefficients, we have $C_{1q}^{\rm NP} = a_L^{\rm NP}(q) + a_R^{\rm NP}(q)$.

To estimate the effect of the K^* resonances on atomic-parity violation, we compute the matching corrections to $a_R^{K^*}(u)$. To this end we evaluate the diagrams with the exchange of a massive vector and a top quark (cf. Fig. 11). The finite part of the contribution of the K^*–top-quark loops, including field renormalization, is

$$a_R^{K^*}(u) = \frac{g_\rho^2 \sin^2\theta_{R,1} \sin^2\theta_{R,3}}{32\pi^2} \times \left[\frac{x^2 - 7x}{8(x-1)} + \frac{3x\log x}{4(x-1)^2} - \frac{x}{4}\log\frac{\mu^2}{m_t^2}\right], \quad (58)$$

where $x \equiv m_t^2/m_{K^*}^2$. Note that the K^* contribution is divergent because of our use of a nongauge vector propagator. The divergent contribution vanishes in the limit $x \to 0$. We estimate the size of the effect by varying the renormalization scale, μ, in the range $[M_{K^*}/2, 2M_{K^*}]$. The same expression also applies for K_1 exchange with $x \to m_t^2/m_{K_1}^2$ and $g_\rho \to g_{a_1}$.

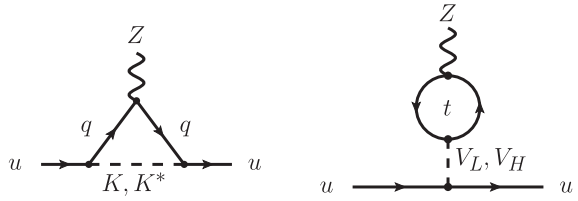

FIG. 11. Vector and pseudoscalar meson contribution to atomic-parity violation.

The effect of HC K exchange is similarly estimated by evaluating the diagram in Fig. 11 with K in the loop. The finite part of the contribution of the K–top-quark loops, including field renormalization, is given by

$$a_R^K(u) = \left(\frac{g_A^{\rm HC}}{f_\pi^{\rm HC}}\right)^2 \frac{\sin^2\theta_{R,1}\sin^2\theta_{R,3}}{32\pi^2} M_K^2 \times \left[\frac{x + x^2}{8(1-x)} + \frac{x\log x}{4(x-1)^2} + \frac{x}{4}\log\frac{\mu^2}{m_t^2}\right], \quad (59)$$

where $x \equiv m_t^2/M_K^2$. Note that this contribution is divergent because of the dimension-5 couplings in Eq. (36). As in the case of the K^* above, the divergent contribution vanishes in the limit $x \to 0$, and the size of the effect is estimated by varying the renormalization scale in the range $[M_K/2, 2M_K]$. All contributions of the K^* and K loops proportional to the weak mixing angle vanish after renormalizing the external fermion fields.

The contribution of the top-quark loop diagram in Fig. 11 (right) is given by

$$a_R^{V_{H,L}}(u) = \mp \frac{g_\rho^2 \sin^2\theta_{R,1}\sin^2\theta_{R,3}}{32\sqrt{2}\pi^2} \sin\theta_{V_{H,L}}^{\rm id} \cos\theta_{V_{H,L}}^{\rm id} \times N_c \left[\frac{m_t^2}{m_{V_{H,L}}^2}\log\frac{\mu^2}{m_t^2}\right]. \quad (60)$$

This is substantially suppressed by the small deviation from the ideal $\omega - \phi$ mixing, $\sin\theta_V^{\rm id} = 0.028$ defined in Eq. (15) (see also Appendix A). The analogous contribution from axial $A_L - A_H$ exchange is obtained by replacing $\theta_{V_{H,L}}^{\rm id} \to \theta_{V,A}^{\rm id}$, $g_\rho \to g_{a_1}$, $m_{V_{H,L}} \to m_{V,A}$. As above, the scale μ in Eq. (60) and the axial-vector analog is varied in the range of half to twice the resonance mass.

Finally, we estimate the effect of the would-be composite quarks on atomic-parity violation. As discussed in Sec. III C, they are closely analogous to a heavy–light meson. In our case the role of the heavy quark is played by the heavy scalar. We thus evaluate the corresponding loops in the UV theory, as shown in Fig. 12. The Z coupling to the scalar is given in terms of the covariant derivative

$$D_\mu = \partial_\mu + \frac{2}{3}\frac{ies_w}{c_w} Z_\mu, \quad (61)$$

in the kinetic term

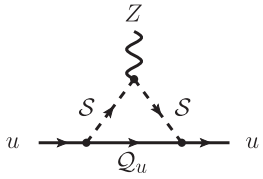

FIG. 12. Contribution of the heavy scalar $\mathcal{S}$ to atomic-parity violation.

$$\mathcal{L}_{\rm kin} = (D_\mu \mathcal{S})^\dagger D^\mu \mathcal{S}. \quad (62)$$

We find that the contribution of the renormalized diagram vanishes.

We can obtain a bound on the size of $a_R^{\rm NP}(u)$ from the measurement of the nuclear weak charge of cesium (^{133}Cs). The contribution of $a_R^{\rm NP}(u)$ to the nuclear weak charge is given by

$$\Delta Q_W = -2(2Z+N)a_R^{\rm NP}(u), \quad (63)$$

where Z and N are the number of protons and neutrons in the nucleus. From the difference of the experimental value, $Q_W^{\rm exp} = -72.58(43)$ [96], and the central value of the SM prediction $Q_W^{\rm SM} = -73.23$ (calculated with input from Ref. [40]),

$$\Delta Q_W({\rm Cs}) \equiv Q_W^{\rm exp}({\rm Cs}) - Q_W^{\rm SM}({\rm Cs}) \subset [0.22, 1.08], \quad (64)$$

we obtain the allowed 1σ region $a_R^{\rm NP}(u) \subset [-0.28, -0.06]\%$. This should be compared with the HC resonance contributions listed in Table XI. One sees that the HC effects are well within the errors on $a_R^{\rm NP}$.

The HC interactions modify the Higgs production cross sections and decays branching ratios. However, we find these modifications to be small in size. The effects of the quartic Higgs coupling to scalar $\mathcal{S}$ are suppressed by its large mass, $m_{\mathcal{S}}$, and are negligible. Modifications of the Higgs couplings to the W and Z arise at loop level and are irrelevant. In principle the partial compositeness of the RH top quark could lead to appreciable modifications in $\bar{t}th$ production, $gg \to h$ fusion, and the $h \to \gamma\gamma$ decay channel, via the RH and LH mixings in Eqs. (29) and (30). The $\bar{t}th$ production cross section is given by

$$\frac{\sigma_{\bar{t}th}^{\rm NP}}{\sigma_{\bar{t}th}^{\rm SM}} = \left(\frac{y_t^{\rm NP}}{y_t^{\rm SM}}\right)^2 \cos\theta_{R3}^2 \cos\theta_{L3}^2 = 1 + \mathcal{O}(1/M^4), \quad (65)$$

where $y_t^{\rm NP} \equiv m_{u_3}/v$ is the top-quark Yukawa coupling in the interaction basis, which differs from the SM relation $y_t^{\rm SM} = m_t^{\rm phys}/v$. Since the physical top-quark mass is given by $m_t^{\rm phys} \simeq m_{u_3} \cos\theta_{R3} \cos\theta_{L3}$, the net change in the $t\bar{t}h$ production cross section is small. Numerically, it is an $\mathcal{O}(1\%)$ effect.

In the limit of a heavy top, where the Higgs low-energy theorem applies, the contributions of the top and the would-be composite top quark u_3' running in the loop completely cancel in the $gg \to h$ and $h \to \gamma\gamma$ amplitudes. The net modifications of the gluon-fusion cross section and the $h \to \gamma\gamma$ branching ratio therefore lie well below a percent.

TABLE XI. Range of the effective a_R coupling to Z in %, induced by the HC resonance contributions discussed in the main text.

	1-σ range [%]
$a_R^K(u)$	$[-0.215, 0.010]$
$a_R^{K^*}(u)$	$[-0.037, -0.005]$
$a_R^{K_1}(u)$	$[-0.054, -0.023]$
$a_R^{V_L}(u)$	$[-0.0008, 0.0009]$
$a_R^{V_H}(u)$	$[-0.0002, 0.0007]$

VI. SIGNALS OF STEALTH STRONG DYNAMICS

Our strong interaction model for enhanced $t\bar{t}$ asymmetries makes several predictions that are not tied to the exact numerical values of the UV parameters and are thus quite robust. It predicts the existence of a tower of resonances that couples strongly to the right-handed top t_R: $K, K^*, K_1, \ldots$. There is a flavor octet of pNGBs: π, K, η (plus the η'), with the lightest state decaying to two jets. The latter is most likely a triplet of pions, with a mass of ~50 GeV. Finally, the minimal form of the model also predicts the existence of a stable, electrically neutral "HC baryon" with a mass of ~250 GeV, which may be searched for in direct dark matter (DM) detection experiments.

The HC resonances $K^*, K_1, \ldots$ decay to $t + j$ final states and are already being searched for, as discussed in Sec. IV E. Their production cross section will increase roughly fourfold in going from the 8-TeV LHC to the 13 TeV LHC; see Table IX. This should be compared with the corresponding approximately fivefold increase in the $t\bar{t}$ cross section. The challenge will be to search for $t + j$ resonances given the larger hadronic activity in 13-TeV events. One could explore the fact that, at 13 TeV, the antitop quarks in $pp \to t + K^* \to t\bar{t}j$ will in general be produced at larger rapidities than the antitop quarks in $t\bar{t}$ events (see Fig. 13). The usefulness of this charge asymmetry at the LHC has been discussed in Ref. [97] for the case of associated $W't$ production.

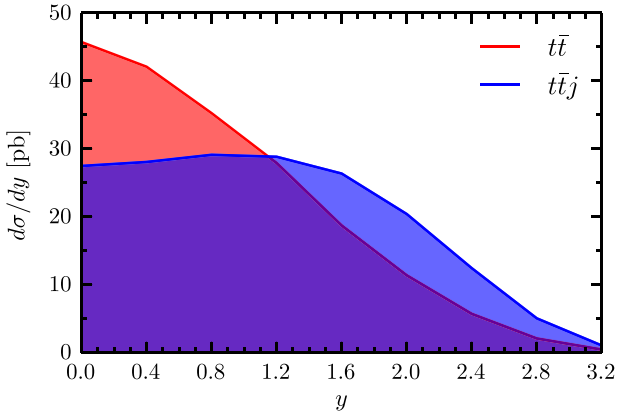

FIG. 13 (color online). The rapidity distribution of the antitop quark from $pp \to t\bar{t}$ (red) and $pp \to tK^* \to t\bar{t}j$ (blue), for LHC at 13 TeV. The $pp \to t\bar{t}j$ differential cross section has been rescaled by a factor 20.

Next, we discuss searches for HC K mesons. A challenge here is that the K decays to an off-shell top, $K \to t^* j$. Ideally, the present experimental searches would be optimized to search not just for $t + j$ resonances but also for $t^* + j$ resonances. Gains are potentially possible, if one allows for softer leptons from the semileptonic decays of the t^*.

The discovery of a light pion decaying to two jets would be a particularly striking signal of stealth strong dynamics. The challenge in searching for HC pions is that they are most copiously produced in decays of higher resonances, which typically results in high-multiplicity final states. An exception is the HC ρ resonance, which almost exclusively decays through $\rho \to \pi\pi$. The s-channel production $pp \to \rho \to \pi\pi$, with $\pi \to 2j$, is effectively already searched for in paired dijet events, as discussed in Sec. IV D. However, in our model both ρ and π are very light, and thus present searches are not sensitive to them. It is unlikely that the sensitivity to the low-mass region can be improved in this type of search at the LHC with increased collision energies. Potentially more promising may be the pair production of ρ resonances, $pp \to \rho\rho \to 4\pi$, in which each pion decays to two jets. Since the ρ's would come primarily from the partonic $u\bar{u} \to \rho\rho$ process, with the u quark in the t-channel, they would have large rapidities.

The cross sections for the process $pp \to \rho\rho$ are 0.38 pb at LHC8 and 1.38 pb at LHC13, respectively. A promising search strategy would thus be to optimize a search for forward pair production of resonances, resulting in two fat jets (potentially further resolved into two jets each using jet substructure techniques).

Finally, our model in its minimal form of Eq. (2) contains a stable neutral HC baryon B_χ formed from three of the light HC quarks. The Lagrangian is invariant under a global $\mathrm{U}(1)_{\mathcal{B}_{\mathrm{HC}}}$ HC baryon-number symmetry, under which the HC quarks $\mathcal{Q}_i$ have charge $\mathcal{B}_{\mathrm{HC}} = 1/3$, $\mathcal{S}$ has charge $\mathcal{B}_{\mathrm{HC}} = -1/3$, while all gauge and SM-matter fields are neutral. Alternatively, one can consider the Z_2^{HC} subgroup, under which the HC quarks and $\mathcal{S}$ are odd, and the SM matter is even. The lightest HC baryon state B_χ ($\mathcal{B}_{\mathrm{HC}} = 1$, or Z_2^{HC} odd) is therefore stable. We estimate its mass by rescaling from QCD, yielding $m_{B_\chi} \sim m_p f_\pi^{\mathrm{HC}}/f_\pi^{\mathrm{HC}} \sim 220$ GeV, not including the HC quark-mass contributions.

Small breaking of the flavor $\mathrm{U}(2)_{U_R}$ symmetry should be accompanied by small mass splittings between the light HC quarks, with $m_{\mathcal{Q}_2} > m_{\mathcal{Q}_1}$ or $m_{\mathcal{Q}_2} < m_{\mathcal{Q}_1}$. We therefore consider two possible flavor structures for the lightest HC baryon, $B_\chi[\mathcal{Q}_1\mathcal{Q}_1\mathcal{Q}_2]$ or $B_\chi[\mathcal{Q}_2\mathcal{Q}_2\mathcal{Q}_1]$, respectively. In general, we expect the two baryons in this "isospin doublet" to be nearly degenerate in mass, since the $\mathrm{U}(2)_{U_R}$ symmetry must remain approximately intact due to flavor changing neutral current constraints.

If B_χ is a thermal relic, its relic abundance is set by its annihilation cross section in the early universe. This is dominated by $B_\chi \bar{B}_\chi \to$ multi-π_{HC} final states. We estimate this by scaling the QCD $p\bar{p}$ annihilation cross section to the HC scale,

$$\sigma_{B_\chi \bar{B}_\chi} \approx \sigma_{p\bar{p}} (f_\pi^{\mathrm{HC}}/f_\pi)^2. \tag{66}$$

The $p\bar{p}$ annihilation cross sections measured by the LEAR collaboration [98] vary from ≈ 200 mb to ≈ 80 mb, for $\bar{p}$ beam momenta varying from 200 MeV to $\approx$600 MeV, respectively. Using Eq. (66) and converting the LEAR $\bar{p}$ beam momenta to center-of-mass values of v/c, we obtain the range of B_χ annihilation cross sections $\sigma_{B_\chi \bar{B}_\chi} \approx 0.01$ mb ($v/c \approx 0.1$) to $\sigma_{B_\chi \bar{B}_\chi} \approx 0.004$ mb ($v/c \approx 0.3$). Note that the nonrelativistic values of v/c are in the range relevant for estimating thermal relic DM abundances. In particular, we find $\langle \sigma_{B_\chi \bar{B}_\chi} v \rangle \sim 3 \times 10^{-20}$ cm^3/s. This is $10^6 \times \langle \sigma v \rangle_{\mathrm{th\,rel}}$, where $\langle \sigma v \rangle_{\mathrm{th\,rel}} = 3 \times 10^{-26}$ cm^3/s would be the annihilation cross section required for B_χ to explain the observed DM abundance.

Our estimate for $\langle \sigma_{B_\chi \bar{B}_\chi} v \rangle$ implies that the B_χ would be a very subleading DM component, with $\Omega_{B_\chi} \sim \mathcal{O}(10^{-6}) \times \Omega_{\mathrm{DM}}$. Nevertheless, DM direct detection searches could be sensitive to it because the B_χ—nucleon scattering cross section is large. The latter is dominated by exchange of the vector mesons $\rho_{\mathrm{HC}}, V_L(\omega_{\mathrm{HC}})$. For simplicity, we only consider the vector couplings $g_V \bar{B}_\chi \gamma_\mu B_\chi V^\mu$ and ignore the higher-dimension tensor couplings. For the coupling strengths, we use the corresponding QCD sum-rule values [99]: $g_\rho = 2.3$ and $g_\omega = 6.9$.

For $B_\chi[\mathcal{Q}_1\mathcal{Q}_1\mathcal{Q}_2]$ its cross section with protons is given by

$$\sigma(B_\chi p \to B_\chi p) = (\kappa_R^\rho)^2 \frac{(g_\rho + g_\omega)^2}{m_{\rho_{\mathrm{HC}}}^4} \frac{m_p^2}{16\pi}, \tag{67}$$

where we have ignored the small splitting between the ρ_{HC} and V_L masses, and the couplings of the ρ_{HC} and V_L to the RH up quark are equal and given by $\kappa_R^\rho = 0.117$; see Table VI. For $B_\chi[\mathcal{Q}_2\mathcal{Q}_2\mathcal{Q}_1]$ its cross section with protons is obtained by substituting $g_\rho \to -g_\rho$ in Eq. (67). In both cases the cross sections with neutrons are a factor of 4 smaller. Thus, for our benchmark we estimate that the B_χ–nucleon cross section would be $\sigma_{\mathrm{scatt}} \sim 10^{-38}$ cm^2 for $B_\chi[\mathcal{Q}_2\mathcal{Q}_2\mathcal{Q}_1]$, and $\sigma_{\mathrm{scatt}} \sim 5 \times 10^{-38}$ cm^2 for $B_\chi[\mathcal{Q}_1\mathcal{Q}_1\mathcal{Q}_2]$. The LUX bound on the DM-nucleon scattering cross section excludes $(\Omega_{B_\chi}/\Omega_{\mathrm{DM}}) \times \sigma_{\mathrm{scatt}} \lesssim 2.5 \times 10^{-45}$ cm^2 [100] for $m_{B_\chi} \sim 220$ GeV. With our estimate for $\Omega_{B_\chi}/\Omega_{\mathrm{DM}}$, the scattering of relic $B_\chi[\mathcal{Q}_2\mathcal{Q}_2\mathcal{Q}_1]$ on nuclei would seem to be at the very limit of the allowed range, whereas for $B_\chi[\mathcal{Q}_1\mathcal{Q}_1\mathcal{Q}_2]$ it is an order of magnitude too large. The uncertainties in our estimates of the B_χ relic density and cross sections with nucleons are large and warrant a more detailed analysis to see whether or not stealth strong dynamics could be discovered in direct DM searches.

Finally, we point out that the HC baryon number (or discrete Z_2^{HC}) symmetry is accidental and therefore may only be approximate. For instance, it could be broken at some higher scale in extensions of our model with a larger field content. In that case all of the HC baryons could be unstable and decay in the early universe. For example, if the SM is extended by a light right-handed neutrino, ν_R, the breaking can exhibit itself through a dimension-7 operator $(\mathcal{S}^\dagger \mathcal{Q}_1 \mathcal{Q}_2) u_R \nu_R$ which also breaks the $\mathrm{U}(2)_{U_R}$ symmetry, where the $\mathrm{SU}(N)_{\mathrm{HC}}$ indices in the bracket are contracted with the antisymmetric Levi-Civitá tensor.

VII. CONCLUSIONS

We have provided an explicit strong interaction model that can produce large enhancements of the $t\bar{t}$ asymmetries at the Tevatron, while not being excluded by other direct or indirect searches for new physics. The model minimally extends the SM field content by a (SM gauge singlet) flavor triplet of vectorlike fermions $\mathcal{Q}_i$ charged under a new strong gauge group, and by a scalar $\mathcal{S}$ charged under QCD, hypercharge and the new strong gauge group. We choose $\mathrm{SU}(3)_{\mathrm{HC}}$ hypercolor for the strong gauge group in order to directly translate the results of QCD strong dynamics, thus reducing the uncertainties in our predictions. An approximate U(2) flavor symmetry is imposed on the fundamental interactions between the hypercolor and SM sectors—the Yukawa-type couplings of the $\mathcal{S}$ to the RH up quarks and $\mathcal{Q}_i$. The $\mathcal{Q}_i$ masses are also U(2) invariant and satisfy a hierarchy analogous to $m_{u,d} \ll m_s \sim f_\pi$ in QCD. The $\mathcal{S}$ is heavier and is thus analogous to a heavy flavor quark in QCD with mass $m \gg 4\pi f_\pi$. The flavor symmetry insures that new physics contributions to flavor-changing neutral currents, e.g. D^0–$\overline{D^0}$ mixing or same-sign top pair production, are negligible or absent. The fact that the HC sector is neutral with respect to the $\mathrm{SU}(2)_L$ weak interaction allows the model to easily evade precision electroweak tests and also ensures that any modifications of the Higgs couplings are very small.

The scale of the new strong dynamics is quite low. The mass of the lightest pseudo-Nambu–Goldstone boson, π_{HC}, is merely 60 GeV, while most of the remaining resonances are in the range of ≈ 150 GeV to ≈ 300 GeV. Despite a plethora of new resonances, the model is, surprisingly, not yet excluded by new physics searches. The reason is twofold: (i) these resonances are bound states of the $\mathcal{Q}_i$ and are thus QCD color neutral, and (ii) the heavier hypercolor scalar $\mathcal{S}$ rapidly decays into high-multiplicity final states, before it can form QCD colored bound states. In particular, pair production of $\mathcal{S}\mathcal{S}^*$ would result in $tj + n$ fat jets or $t\bar{t} + n$ fat jets final states, where a fat jet is associated with a $\pi_{\mathrm{HC}} \to jj$ or $K_{\mathrm{HC}} \to t^* j$ decay.

There already has been considerable progress at the LHC in searches for new physics involving final states with large jet multiplicities. However, searches in relatively low-multiplicity final states, including fat jets, are probably the most promising for discovery of hypercolor resonances. An example is pair production of ρ_{HC} resonances, with each ρ_{HC} decaying to a pair of HC pions, resulting in the chain $pp \to \rho_{\mathrm{HC}}\rho_{\mathrm{HC}} \to 4\pi_{\mathrm{HC}} \to 4$ fat jets. The rather strong coupling of the hypercolor sector to the top quarks leads to observable $t\bar{t}$ charge asymmetries in associated hypercolor resonance production at the LHC. This feature could be useful in discriminating signal from background in $t +$ jet resonance searches. For example, the $\bar{t}$ in the process $pp \to tK^*_{\mathrm{HC}} \to t\bar{t}j$ is produced with relatively large rapidities compared to the top and compared to the antitop in $pp \to t\bar{t}$. This feature could also be useful in virtual $t^* + j$ resonance searches associated with the process $pp \to tK_{\mathrm{HC}} \to t\bar{t}^* j$.

We have used known nonperturbative aspects of QCD, as well as familiar approximations like QCD sum rules, vector-meson dominance, and a naive quark model, combined with simple scaling arguments to obtain reasonable estimates of the resonance masses and interaction strengths in our QCD-like hypercolor model. An interesting application concerns the relic abundance of the lightest HC baryon, B_χ. If the accidental HC baryon number symmetry of our Lagrangian is left unbroken by higher-dimensional operators involving additional light non-SM fields, then the B_χ is stable. Scaling the measured low-energy QCD $p\bar{p}$ annihilation cross sections will imply a B_χ relic abundance that is only $\mathcal{O}(10^{-6})$ as large as the observed dark matter abundance. Nevertheless, the B_χ-nucleon cross section is large enough to be close to saturating the present direct dark matter detection bounds and may yield an observable signal in the next generation of the dark matter direct detection experiments or rule out a stable B_χ.

An interesting open question is also the UV structure of our model. The one-loop running of the Yukawa couplings h_1, h_3 and the HC gauge coupling g_{HC} gives a Landau pole at $\mu = O(\text{few TeV})$, whereas two-loop RGEs give an approximate UV fixed point for h_3 of nonperturbative strength, $h_3^* \approx 8$, that is realized at $\mu = O(10\ \text{TeV})$, with h_1 and g_{HC} asymptotically free. To settle the question which of the two possibilities is realized would require nonperturbative methods, and is beyond the scope of the current work, but could be an interesting future research direction.

In summary, the presented model can lead to large $t\bar{t}$ asymmetry at the Tevatron and evades present experimental bounds but can be searched for with improved strategies at the LHC and in direct dark matter detection experiments.

ACKNOWLEDGMENTS

J. B. and E. S. would like thank Antonio Pich for useful discussions. We would like to thank the Weizmann Institute Phenomenology group and the CERN theory group for their warm hospitality during various stages of this work. A. K. and J. B. are supported by DOE Grant No. FG02-84-ER40153. J. Z. and J. B. are supported by the U.S. National Science Foundation under CAREER Grant

No. PHY-1151392. E. S. is supported by the DFG cluster of excellence "Origin and Structure of the Universe." We also thank the Aspen Center for Physics, supported by the NSF Grant No. 1066293, and the KITP, supported in part by the National Science Foundation under Grant No. NSF PHY11-25915, for their warm hospitality. A. K. and J. Z. are grateful to the Mainz Institute for Theoretical Physics for its hospitality and its partial support during the completion of this work. E. S. would like to thank the Department of Physics at University of Cincinnati for its warm hospitality during the initial stages of this work.

APPENDIX A: RESONANCE MASS SPECTRA

The masses of the HC mesons are obtained from the measured spectrum of QCD mesons by appropriate rescalings. To good approximation, the QCD ρ mass, $m_\rho^{\rm QCD}$, corresponds to the massless limit of the HC ρ meson, $M_\chi = \lim_{m_{\mathcal{Q}_i}\to 0} m_\rho^{\rm HC}$. In obtaining the spectra, we also need to allow for variations of the HC quark masses. We do this by employing chiral perturbation theory (ChPT) for the pseudoscalar mesons and a naive quark model for the vector and axial-vector resonances.

1. Pseudoscalar mesons

The compositions of the HC pion and kaon in terms of the HC quarks are

$$\begin{aligned}|\pi^{1(2)}\rangle &= |\bar{\mathcal{Q}}_{1(2)}\mathcal{Q}_{2(1)}\rangle,\\ |\pi^3\rangle &= \frac{1}{\sqrt{2}}(|\bar{\mathcal{Q}}_1\mathcal{Q}_1\rangle - |\bar{\mathcal{Q}}_2\mathcal{Q}_2\rangle),\\ |K^{1(2)}\rangle &= |\bar{\mathcal{Q}}_{1(2)}\mathcal{Q}_3\rangle,\\ |\bar{K}^{1(2)}\rangle &= |\bar{\mathcal{Q}}_3\mathcal{Q}_{1(2)}\rangle,\end{aligned} \tag{A1}$$

while the octet and the singlet pseudoscalars are given by

$$\begin{aligned}|\eta_8\rangle &= \frac{1}{\sqrt{6}}(|\bar{\mathcal{Q}}_1\mathcal{Q}_1\rangle + |\bar{\mathcal{Q}}_2\mathcal{Q}_2\rangle - 2|\bar{\mathcal{Q}}_3\mathcal{Q}_3\rangle),\\ |\eta_0\rangle &= \frac{1}{\sqrt{3}}(|\bar{\mathcal{Q}}_1\mathcal{Q}_1\rangle + |\bar{\mathcal{Q}}_2\mathcal{Q}_2\rangle + |\bar{\mathcal{Q}}_3\mathcal{Q}_3\rangle).\end{aligned} \tag{A2}$$

As explained in the main text, we neglect $\eta - \eta'$ mixing so that the $\eta_8 = \eta$ and $\eta_0 = \eta'$.

The quadratic terms in the chiral Lagrangian yield expressions for the squared pseudoscalar masses which are linear in the quark masses,

$$\begin{aligned}(m_{\pi^{1,2,3}})^2 &= k_f \frac{M_\chi}{m_\rho^{\rm QCD}} 2m_{\mathcal{Q}_1},\\ (m_{K^{1,2},\bar{K}^{1,2}})^2 &= k_f \frac{M_\chi}{m_\rho^{\rm QCD}}(m_{\mathcal{Q}_1} + m_{\mathcal{Q}_3}),\\ (m_\eta)^2 &= k_f \frac{M_\chi}{m_\rho^{\rm QCD}}\frac{2}{3}(m_{\mathcal{Q}_1} + 2m_{\mathcal{Q}_3}).\end{aligned} \tag{A3}$$

We use $k_f = 2.765$ as obtained from the lattice QCD calculation in Ref. [101]. The η' is assumed to be much heavier than the other pseudoscalar mesons and is omitted from our analysis as explained in Sec. III A.

2. Vector mesons

The vector-meson masses and the mixing angle between the flavor-singlet and octet states are calculated using the naive quark-model approach in Ref. [41]. The decompositions of the ρ and K^* in terms of HC quark states are

$$\begin{aligned}|\rho^{1(2)}\rangle &= |\bar{\mathcal{Q}}_{1(2)}\mathcal{Q}_{2(1)}\rangle,\\ |\rho^3\rangle &= \frac{1}{\sqrt{2}}(|\bar{\mathcal{Q}}_1\mathcal{Q}_1\rangle - |\bar{\mathcal{Q}}_2\mathcal{Q}_2\rangle),\\ |K^{*1(2)}\rangle &= |\bar{\mathcal{Q}}_{1(2)}\mathcal{Q}_3\rangle, \qquad |\bar{K}^{*1(2)}\rangle = |\bar{\mathcal{Q}}_3\mathcal{Q}_{1(2)}\rangle.\end{aligned} \tag{A4}$$

Their masses are given by

$$\begin{aligned}(m_{\rho^{1,2,3}})^2 &= \mu_V^{\rm HC}(E_{0,V}^{\rm HC} + 2m_{\mathcal{Q}_1}),\\ (m_{K^{*1,2},\bar{K}^{*1,2}})^2 &= \mu_V^{\rm HC}(E_{0,V}^{\rm HC} + m_{\mathcal{Q}_3} + m_{\mathcal{Q}_1}).\end{aligned} \tag{A5}$$

Here, $\mu_V^{\rm HC}$ is an overall mass-scale parameter, $E_{0,V}$ describes the binding energy in the limit of massless HC quarks, while the $m_{\mathcal{Q}_i}$ are the HC quark masses.

The octet and singlet vector-meson states are

$$\begin{aligned}|V_8\rangle &= \frac{1}{\sqrt{6}}(|\bar{\mathcal{Q}}_1\mathcal{Q}_1\rangle + |\bar{\mathcal{Q}}_2\mathcal{Q}_2\rangle - 2|\bar{\mathcal{Q}}_3\mathcal{Q}_3\rangle),\\ |V_0\rangle &= \frac{1}{\sqrt{3}}(|\bar{\mathcal{Q}}_1\mathcal{Q}_1\rangle + |\bar{\mathcal{Q}}_2\mathcal{Q}_2\rangle + |\bar{\mathcal{Q}}_3\mathcal{Q}_3\rangle).\end{aligned} \tag{A6}$$

The mixing angle between the flavor-singlet and octet vector mesons is obtained by diagonalizing the corresponding mass matrix

$$\begin{pmatrix}(m_{V_L})^2 & 0\\ 0 & (m_{V_H})^2\end{pmatrix} = R_V \begin{pmatrix}\mu_V^{\rm HC}(E_{0V}^{\rm HC} + \frac{2}{3}(2m_{\mathcal{Q}_1} + m_{\mathcal{Q}_3}) + x_{\rm an,V}^{\rm HC}) & -\frac{2}{3}\sqrt{2}\mu_V^{\rm HC}(m_{\mathcal{Q}_3} - m_{\mathcal{Q}_1})\\ -\frac{2}{3}\sqrt{2}\mu_V^{\rm HC}(m_{\mathcal{Q}_3} - m_{\mathcal{Q}_1}) & \mu_V^{\rm HC}(E_{0V}^{\rm HC} + \frac{2}{3}(m_{\mathcal{Q}_1} + 2m_{\mathcal{Q}_3}))\end{pmatrix} R_V^{-1}, \tag{A7}$$

where $V_{L,H}$ are the mass eigenstates. The mass matrix on the rhs is given in the $V_0 - V_8$ basis. It contains an additional parameter $x_{\rm an,V}^{\rm HC}$ which takes into account the annihilation of the flavor-singlet meson into gluonic intermediate states. The matrix R_V is chosen to diagonalize the mixing matrix and thereby yields the mixing angle,

$$\begin{pmatrix} |V_L\rangle \\ |V_H\rangle \end{pmatrix} = R_V \begin{pmatrix} |V_0\rangle \\ |V_8\rangle \end{pmatrix} = \begin{pmatrix} \cos\theta_V & \sin\theta_V \\ -\sin\theta_V & \cos\theta_V \end{pmatrix} \begin{pmatrix} |V_0\rangle \\ |V_8\rangle \end{pmatrix}. \tag{A8}$$

We first fit the parameters of the ansatz in Eq. (A7), applied to QCD. Our inputs are the measured QCD vector-meson masses, the mixing angle $\theta_V^{\rm QCD} = 38.7°$, and the light-quark masses $m_u = m_d = 4$ MeV, $m_s = 100$ MeV. They yield

$$\begin{aligned} &\mu_V^{\rm QCD} = 2.21 \text{ GeV}, \qquad E_{0,V}^{\rm QCD} = 260 \text{ MeV}, \\ &x_{{\rm an},V}^{\rm QCD} = 15 \text{ MeV}, \end{aligned} \tag{A9}$$

where we only quote the central values. This suffices since the errors are much smaller than the errors we ascribe to the extrapolation to the HC case. The HC parameters are obtained by rescaling in the usual way

$$\{\mu_V^{\rm HC}, E_{0,V}^{\rm HX}, x_{{\rm an,V}}^{\rm HC}\} = \frac{M_\chi}{m_\rho^{\rm QCD}} \{\mu_V^{\rm QCD}, E_{0,V}^{\rm QCD}, x_{\rm an,V}^{\rm QCD}\}. \tag{A10}$$

Note that $M_\chi = \sqrt{\mu_V^{\rm HC} E_{0,V}^{\rm HC}}$.

The mixing angle is close to ideal. The deviation from ideal mixing is parametrized by the angle $\theta_V^{\rm id}$; see the definition in Eq. (16). It is related to θ_V as

$$\sin\theta_V^{\rm id} = -\frac{1}{\sqrt{3}}\cos\theta_V + \sqrt{\frac{2}{3}}\sin\theta_V. \tag{A11}$$

The singlet–octet mixing angle θ_V is directly related to $x_{{\rm an,V}}^{\rm HC}$ as [41]

$$\tan 2\theta_V = 2\frac{\sqrt{N_f - 1}}{N_f - 2 - \xi_V}, \tag{A12}$$

with

$$\xi_V = \frac{N_f x_{{\rm an,V}}^{\rm HC}}{2(m_{\mathcal{Q}_3} - m_{\mathcal{Q}_1})} \tag{A13}$$

and $N_f = 3$ in our HC model. Note in particular that $x_{{\rm an,V}}^{\rm HC} = 0$ corresponds to ideal mixing, $\theta_V^{\rm id} = 0$.

3. Axial vectors

The same naive quark model [41] can also be applied to the axial ($^3P_1$) vector masses. The decompositions of the a_1 and K_1 in terms of HC quark states are

$$\begin{aligned} |a_1^{1(2)}\rangle &= |\bar{\mathcal{Q}}_{1(2)}\mathcal{Q}_{2(1)}\rangle, \\ |a_1^3\rangle &= \frac{1}{\sqrt{2}}(|\bar{\mathcal{Q}}_1\mathcal{Q}_1\rangle - |\bar{\mathcal{Q}}_2\mathcal{Q}_2\rangle), \\ |K_1^{1(2)}\rangle &= |\bar{\mathcal{Q}}_{1(2)}\mathcal{Q}_3\rangle, \qquad |\bar{K}_1^{1(2)}\rangle = |\bar{\mathcal{Q}}_3\mathcal{Q}_{1(2)}\rangle. \end{aligned} \tag{A14}$$

Note that we have ignored the $^1P_1$ multiplet and the corresponding K_{1A}-K_{2A} mixing, as explained in the main text. The naive quark-model parameters are now $\mu_A^{\rm HC}$, $E_{0,A}^{\rm HC}$, and $x_{{\rm an,A}}^{\rm HC}$. The a_1 and K_1 masses are given by

$$\begin{aligned} (M_{a_1^{1,2,3}}^{\rm HC})^2 &= \mu_A^{\rm HC}(E_{0,A}^{\rm HC} + 2m_{\mathcal{Q}_1}), \\ (M_{K_1^{1,2}}^{\rm HC})^2 &= \mu_A^{\rm HC}(E_{0,A}^{\rm HC} + m_{\mathcal{Q}_3} + m_{\mathcal{Q}_1}). \end{aligned} \tag{A15}$$

The description of the $A_0 - A_8$ (singlet-octet) system is given by substituting $V \to A$ in Eqs. (A6)–(A8) and (A11)–(A13). The mass eigenstates are denoted by A_L and A_H.

The quark-model parameters in QCD are obtained by fitting to the a_1, K_{1A}, $f_1(1420)$, $f_1(1285)$ masses and the mixing angle $\theta_A^{\rm id}$. For the mixing angle, we inflate the errors, taking $\theta_A^{\rm id} = (23.0 \pm 23.0)°$ (a recent LHCb determination [102] obtains $\pm(24^{+3.1+0.6}_{-2.6-0.8})°$, and recent lattice determinations in Ref. [103] range from $\pm[25, 36]°$). This gives

$$\begin{aligned} &\mu_A^{\rm QCD} = 2.16 \text{ GeV}, \qquad E_{0,A}^{\rm QCD} = 700 \text{ MeV}, \\ &x_{{\rm an},A}^{\rm QCD} = 64 \text{ MeV}, \end{aligned} \tag{A16}$$

where again we only quote the central values.

4. Would-be composite quarks u'

The would-be composite quarks, $u_i' \sim [\mathcal{S}\mathcal{Q}_i]$, can be thought of as analogs of a heavy–light vector meson, as discussed in Sec. III C. Carrying over the expression for the heavy–light meson masses in the heavy-quark limit in QCD to our would-be composite quarks gives $M_{u_i'} = \mathcal{O}(\Lambda_{\rm HC}) + m_{\mathcal{Q}_i} + m_{\mathcal{S}}$. Here, $\Lambda_{\rm HC}$ is the HC confinement scale. The scalar $\mathcal{S}$ corresponds to a QCD heavy quark with mass between that of the charm and the bottom quark. We thus estimate the HC-dynamics contribution to the u_i' mass to be roughly the ρ mass, similarly to what is found for the D and B mesons in QCD. We set the would-be HC quark masses to

$$\begin{aligned} M_{u'} &= M_{c'} = M_\chi + m_{\mathcal{Q}_1} + m_{\mathcal{S}}, \\ M_{t'} &= M_\chi + m_{\mathcal{Q}_3} + m_{\mathcal{S}}. \end{aligned} \tag{A17}$$

For our benchmark this gives $M_{u',c'} = 691$ GeV and $M_{t'} = 718$ GeV.

APPENDIX B: DECAY CONSTANTS AND COUPLINGS

In this Appendix we explain in more detail how we obtain our estimates for the couplings of the HC resonances to the would-be composite quarks and our estimates for the decay constants of the would-be composite quarks.

We start with the VMD estimates of the HC resonance couplings to the would-be composite quarks, Eq. (31). The VMD assumption states that the matrix element $\langle u'|J^{a\mu}|u'\rangle$, where $J^{a\mu} = \bar{\mathcal{Q}}_i \gamma^\mu (T^a)_{ij} \mathcal{Q}_j$, is dominated by the lowest-lying vector resonance V^a with the same quantum numbers as the current $J^{a\mu}$. For appropriately chosen linear combinations of the flavor-group generators, T^a, these will be the vector resonances ρ, ω, K^*, ϕ. In the VMD limit, we can write

$$\langle u'|J^{a\mu}|u'\rangle \to \langle u'|u'V^a\rangle \frac{1}{q^2 - M_V^2} \langle V^a|J^{a\mu}|0\rangle. \tag{B1}$$

Using the definitions in Eqs. (8) and (31), we have

$$\langle u'|J^{a\mu}|u'\rangle \to g_V \frac{f_V M_V}{q^2 - M_V^2} \bar{u}' T^a \gamma_\mu u', \tag{B2}$$

where we have used $\sum \epsilon_\mu \epsilon_\nu^* = g_{\mu\nu} + q_\mu q_\nu / M_V^2$ and the Dirac equation. On the other hand, the vector current matrix element can also be written in terms of the form factors

$$\langle u'|J^{a\mu}|u'\rangle = \bar{u}' T^a [\gamma_\mu f_1(q^2) + \frac{i\sigma_{\mu\nu}}{2m_{u'}} q^\nu f_2(q^2)] u', \tag{B3}$$

where the normalization condition is $f_1(0) = 1$. Equating the last two expressions for $q^2 \to 0$ leads to the VMD relation

$$g_V = \frac{M_V}{f_V}. \tag{B4}$$

Next, we describe the determination of the decay constant, $f_{u'}$, of the would-be composite quarks. In this estimate we can take the $\bar{q}_i$ to be massless and focus entirely on the $m_{\mathcal{S}}$ dependence of $f_{u'}$. Again we are guided by QCD. For $m_{\mathcal{S}} \ll M_\chi$ (i.e. $m_q \ll m_\rho$ in QCD) we use the fact that ChPT and lattice QCD simulations show a linear dependence: $f_{u'} = a(f_{u'})_0 + b m_{\mathcal{S}}$. For heavy $m_{\mathcal{S}} \gg M_\chi$, HQET yields the scaling $f_{u'} = c/\sqrt{m_{\mathcal{S}}}$ [104,105]. Rescaling from QCD yields an expression for $f_{u'}^{\rm HC}$ of the form

$$f_{u'}^{\rm HC} = f_\rho^{\rm QCD} \frac{M_\chi}{M_\rho^{\rm QCD}} \mathcal{F}\left(\frac{m_{u'}}{M_\chi}\right), \tag{B5}$$

where we use the fact that the would-be composite quark u' most closely resembles the ρ in QCD (i.e. it is a low-lying resonance but not a pNGB). The dimensionless function

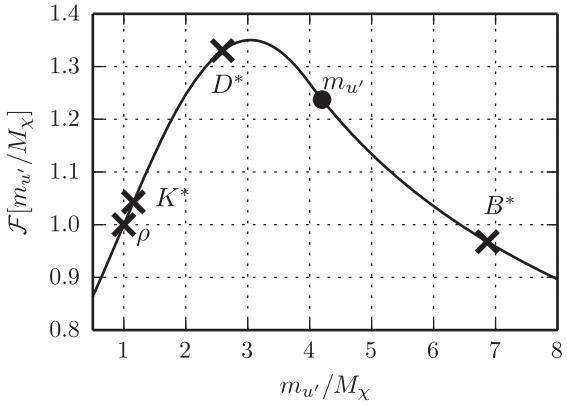

FIG. 14. The normalized interpolating function $\mathcal{F}$ used to estimate the decay constant $f_{u'}$ as a function of the dimensionless quantity $m_{u'}/M_\chi$. The function $\mathcal{F}$ is chosen such that it reproduces the measured QCD decay constants f_ρ, f_{K^*}, f_{D^*}, f_{B^*}, denoted with crosses. The value of $m_{u'}$ used in the benchmark is denoted by a circle.

$\mathcal{F}(x)$ captures the ChPT and heavy quark effective theory (HQET) behaviors. For $x \to 0$ we have $\mathcal{F}(x) = c\mathcal{F}(0) + \mathcal{F}(0)'x$, while for $x \gg 1$ we have $\mathcal{F}(x) = \mathcal{F}_\infty/\sqrt{x}$. The constant $\mathcal{F}_\infty$ is determined from the value of f_{B^*} in QCD. The HQET form of $\mathcal{F}(x)$ is assumed to be valid above $x_{\rm match} = m_{u'}/M_\chi \simeq 4.1$, and a quadratic interpolation is used for lower values of x, such that the QCD values of f_{D^*}, f_{K^*}, and f_ρ are all properly described. The result is shown in Fig. 14. For our estimates of $f_{u'}$, only the HQET scaling turns out to be needed (along with the proper rescaling to the HC scale), given the range of masses we considered for $m_{\mathcal{S}}$.

APPENDIX C: DECAY WIDTHS

The decay widths for ρ and K^* decays to pseudoscalar pairs are given by

$$\begin{aligned}
\frac{\Gamma_\rho}{m_\rho} &= \frac{1}{96\pi}\left[2g_{\rho\pi\pi}^2\left(1 - \frac{4m_\pi^2}{m_\rho^2}\right)^{3/2} + g_{\rho KK}^2\left(1 - \frac{4m_K^2}{m_\rho^2}\right)^{3/2}\right], \\
\frac{\Gamma_{K^*}}{m_{K^*}} &= \frac{g_{K^*K\pi}^2}{64\pi}\left[f_{\rm PS}\left(\frac{m_\pi}{m_{K^*}}, \frac{m_K}{m_{K^*}}\right)\right]^3 \\
&\quad + \frac{g_{K^*K\eta_8}^2}{64\pi}\left[f_{\rm PS}\left(\frac{m_{\eta_8}}{m_{K^*}}, \frac{m_K}{m_{K^*}}\right)\right]^3.
\end{aligned} \tag{C1}$$

Here, the phase-space function is defined as

$$f_{\rm PS}(x, y) = 1 - 2x^2 - 2y^2. \tag{C2}$$

Note that, due to flavor-symmetry breaking, the effective couplings $g_{\rho KK}$, $g_{K^*K\pi}$, $g_{K^*K\eta_8}$ could differ from $g_{\rho\pi\pi}$, defined in the flavor-symmetric limit in Eq. (14). In our numerics we take, however, all of them equal to the VMD value g_ρ, as discussed in Sec. III B.

The decay widths of V_L and V_H read

$$\frac{\Gamma_{V_L}}{m_{V_L}} = \frac{g_\rho^2}{32\pi}\sin^2\theta_V\left(1-4\frac{m_K^2}{m_{V_L}^2}\right)^{3/2},$$
$$\frac{\Gamma_{V_H}}{m_{V_H}} = \frac{g_\rho^2}{32\pi}\cos^2\theta_V\left(1-4\frac{m_K^2}{m_{V_H}^2}\right)^{3/2}, \quad \text{(C3)}$$

where θ_V is the mixing angle in Eq. (A8), and we have used the VMD estimate of the effective coupling.

The partial widths of the vector mesons to SM quarks are governed by their mixing with the would-be composite quarks; see Eq. (33). For instance, the $\bar{K}^{*1} \to \bar{t}u$ partial decay width is given by

$$\frac{\Gamma_{\bar{K}^{*1}\to\bar{t}u}}{M_{K^*}} = \frac{1}{16\pi}f_{\rm PS}\left(0,\frac{m_t}{m_{K^*}}\right)[(\lambda_{13}^R)^2+(\lambda_{13}^L)^2] \times\left[1-\frac{m_t^2}{2m_{K^*}^2}-\frac{1}{2}\left(\frac{m_t^2}{m_{K^*}^2}\right)^2\right] \quad \text{(C4)}$$

and similarly for $\Gamma_{\bar{K}^{*2}\to\bar{t}c}$ with $\lambda_{13}^{L/R}\to\lambda_{23}^{L/R}$.

The ${}^3P_1$ axial vectors can have $A \to VP$ decays and, if kinematically allowed, $A \to VV$ decays. The former usually dominate. To estimate the corresponding decay widths, we follow the phenomenological analysis for $A \to VP$ decays in QCD given in Ref. [42] and carried out in the SU(3) limit. The authors point out that in general one can express the decay amplitudes in terms of two independent operators,

$$\langle A_{\mu\nu}[V^{\mu\nu},P]\rangle, \langle A_\mu[V^\mu,P]\rangle. \quad \text{(C5)}$$

They only choose the first operator for their study, which involves the tensor representations for the vector operators. However, they explain that an analysis involving only the second operator would yield similar results. The $A \to VP$ Lagrangian, in the SU(3) limit, is then

$$\mathcal{L}_{AVP} = i\tilde{F}\langle A_{\mu\nu}[V^{\mu\nu},P]\rangle, \quad \text{(C6)}$$

where $\langle\ldots\rangle$ denotes a trace over the SU(3) generators, $\tilde{F}$ is a dimensionful coupling, and the factor i insures that the Lagrangian is Hermitian. The tensor-field operators $V_{\mu\nu}$ is normalized such that

$$\langle 0|V_{\mu\nu}|V(P,\epsilon)\rangle = \frac{i}{M_V}(P_\mu\epsilon_\nu - P_\nu\epsilon_\mu) \quad \text{(C7)}$$

and similarly for $A_{\mu\nu}$.

The partial decay widths of the axial vectors are then given by

$$\Gamma_{A\to VP} = \frac{|\lambda_{AVP}|^2}{2\pi}\frac{\tilde{F}^2 q}{m_A^2}\left(1+\frac{2}{3}\frac{q^2}{m_V^2}\right), \quad \text{(C8)}$$

where $q = f_{\rm PS}(m_V^2/m_A^2, m_P^2/m_A^2)\cdot 1/(2m_A)$ and λ_{AVP} are decay-mode-specific dimensionless prefactors. For instance, the mixed flavor octet-singlet states A_L and A_H decay to K^*K final states. Summing over the $K^{*\pm}K^\mp$, $K^{*0}\bar{K}^0$, and $\bar{K}^{*0}K^0$ decay modes, the $A_L \to K^*K$ and $A_H \to K^*K$ decay widths are obtained by using the expression

$$\lambda_{A_{L,H}K^*K} = 2\left(\frac{\cos^2\theta_{\rm A}^{\rm id}}{2}+\sin^2\theta_{\rm A}^{\rm id}\pm\sqrt{2}\sin\theta_{\rm A}^{\rm id}\cos\theta_{\rm A}^{\rm id}\right)^{1/2}, \quad \text{(C9)}$$

for the λ prefactor in Eq. (C8)

The a_1 decays to $\rho\pi$ and K^*K. Summing over these final states, the $a_1 \to \rho\pi$ and $a_1 \to K^*K$ partial decay widths are obtained by using

$$\lambda_{a_1\rho\pi} = 2 \quad \text{and} \quad \lambda_{a_1K*K} = \sqrt{2} \quad \text{(C10)}$$

in Eq. (C8). The $K_1 \to \rho K, K^*\pi, K\omega, K\phi$ partial decay widths follow from Eq. (C8) using

$$\lambda_{K_1\rho K, K_1\pi K^*} = \sqrt{\frac{3}{2}}, \qquad \lambda_{K_1\omega K} = \frac{1}{\sqrt{2}}, \qquad \lambda_{K_1\phi K} = 1. \quad \text{(C11)}$$

The fits to the QCD axial-vector decay widths yield a large allowed range for $\tilde{F}$. In particular, the solutions for $\tilde{F}$ vary from $\tilde{F}_{\rm QCD} \approx 1200$ MeV to $\tilde{F}_{\rm QCD} \approx 1600$ MeV. We rescale from QCD with the usual scale factor,

$$\tilde{F}_{\rm HC} = \frac{M_\chi}{m_{\rho^{\rm QCD}}}\tilde{F}_{\rm QCD}. \quad \text{(C12)}$$

Finally, we quote the total decay width of the heavy scalar $\mathcal{S}$, including the phase-space factors

$$\frac{\Gamma_{\mathcal{S}\to u_i\bar{\mathcal{Q}}_i}}{m_{\mathcal{S}}} = \frac{|h_i|^2}{16\pi}f_{\rm PS}\left(\frac{m_{u_i}}{m_{\mathcal{S}}},\frac{m_{\mathcal{Q}_i}}{m_{\mathcal{S}}}\right)\left(1-\frac{m_{u_i}^2}{m_{\mathcal{S}}^2}-\frac{m_{\mathcal{Q}_i}^2}{m_{\mathcal{S}}^2}\right). \quad \text{(C13)}$$

[1] E. H. Simmons, Nucl. Phys. **B312**, 253 (1989).
[2] S. Samuel, Nucl. Phys. **B347**, 625 (1990).
[3] M. Dine, A. Kagan, and S. Samuel, Phys. Lett. B **243**, 250 (1990).
[4] C. D. Carone and E. H. Simmons, Nucl. Phys. **B397**, 591 (1993).
[5] C. D. Carone and H. Georgi, Phys. Rev. D **49**, 1427 (1994).
[6] A. L. Kagan, in 2008 KITP workshop on Physics of the Large Hadron Collider, LOCATION, 2008 (unpublished), http://online.itp.ucsb.edu/online/lhc08/kagan/.
[7] M. Antola, M. Heikinheimo, F. Sannino, and K. Tuominen, J. High Energy Phys. 03 (2010) 050.
[8] A. Azatov, J. Galloway, and M. A. Luty, Phys. Rev. Lett. **108**, 041802 (2012).
[9] A. Azatov, J. Galloway, and M. A. Luty, Phys. Rev. D **85**, 015018 (2012).
[10] M. J. Strassler and K. M. Zurek, Phys. Lett. B **651**, 374 (2007).
[11] T. Han, Z. Si, K. M. Zurek, and M. J. Strassler, J. High Energy Phys. 07 (2008) 008.
[12] L. B. Okun, Pisma Zh.Eksp.Teor.Fiz. **31**, 156 (1979) [**31**, 144 (1980)].
[13] L. Okun, Nucl. Phys. **B173**, 1 (1980).
[14] J. Kang and M. A. Luty, J. High Energy Phys. 11 (2009) 065.
[15] G. D. Kribs, T. S. Roy, J. Terning, and K. M. Zurek, Phys. Rev. D **81**, 095001 (2010).
[16] G. Burdman, Z. Chacko, H.-S. Goh, R. Harnik, and C. A. Krenke, Phys. Rev. D **78**, 075028 (2008).
[17] R. Harnik and T. Wizansky, Phys. Rev. D **80**, 075015 (2009).
[18] S. P. Martin, Phys. Rev. D **83**, 035019 (2011).
[19] C. Kilic, T. Okui, and R. Sundrum, J. High Energy Phys. 07 (2008) 038.
[20] C. Kilic, S. Schumann, and M. Son, J. High Energy Phys. 04 (2009) 128.
[21] C. Kilic, T. Okui, and R. Sundrum, J. High Energy Phys. 02 (2010) 018.
[22] C. Kilic and T. Okui, J. High Energy Phys. 04 (2010) 128.
[23] J. F. Kamenik, J. Shu, and J. Zupan, Eur. Phys. J. C **72**, 2102 (2012).
[24] B. Grinstein, A. L. Kagan, M. Trott, and J. Zupan, Phys. Rev. Lett. **107**, 012002 (2011).
[25] B. Grinstein, A. L. Kagan, J. Zupan, and M. Trott, J. High Energy Phys. 10 (2011) 072.
[26] M. I. Gresham, I. -W. Kim, and K. M. Zurek, Phys. Rev. D **85**, 014022 (2012).
[27] J. Aguilar-Saavedra and M. Perez-Victoria, J. High Energy Phys. 09 (2011) 097.
[28] B. Grinstein, M. Redi, and G. Villadoro, J. High Energy Phys. 11 (2010) 067.
[29] P. Ko, Y. Omura, and C. Yu, Phys. Rev. D **85**, 115010 (2012).
[30] S. Jung, H. Murayama, A. Pierce, and J. D. Wells, Phys. Rev. D **81**, 015004 (2010).
[31] Y. Cui, Z. Han, and M. D. Schwartz, J. High Energy Phys. 07 (2011) 127.
[32] K. Blum, Y. Hochberg, and Y. Nir, J. High Energy Phys. 10 (2011) 124.
[33] J. Drobnak, A. L. Kagan, J. F. Kamenik, G. Perez, and J. Zupan, Phys. Rev. D **86**, 094040 (2012).
[34] J. Adelman, J. Ferrando, and C. White, J. High Energy Phys. 02 (2013) 091.
[35] Y. Grossman, Y. Nir, J. Thaler, T. Volansky, and J. Zupan, Phys. Rev. D **76**, 096006 (2007).
[36] C. McNeile, A. Bazavov, C. T. H. Davies, R. J. Dowdall, K. Hornbostel, G. P. Lepage, and H. D. Trottier, Phys. Rev. D **87**, 034503 (2013).
[37] M. Beneke, J. Rohrer, and D. Yang, Nucl. Phys. **B774**, 64 (2007).
[38] K.-C. Yang, Nucl. Phys. **B776**, 187 (2007).
[39] N. Isgur, C. Morningstar, and C. Reader, Phys. Rev. D **39**, 1357 (1989).
[40] J. Beringer *et al.* (Particle Data Group), Phys. Rev. D **86**, 010001 (2012).
[41] H.-Y. Cheng and R. Shrock, Phys. Rev. D **84**, 094008 (2011).
[42] L. Roca, J. Palomar, and E. Oset, Phys. Rev. D **70**, 094006 (2004).
[43] A. Abada, D. Bećirević, P. Boucaud, G. Herdoiza, J. P. Leroy, A. Le Yaouanc, and O. Pène, J. High Energy Phys. 02 (2004) 016.
[44] H. Ohki, H. Matsufuru, and T. Onogi, Phys. Rev. D **77**, 094509 (2008).
[45] B. El-Bennich, M. A. Ivanov, and C. D. Roberts, Phys. Rev. C **83**, 025205 (2011).
[46] T. Aaltonen *et al.* (CDF Collaboration), Phys. Rev. D **87**, 092002 (2013).
[47] V. M. Abazov *et al.* (D0 Collaboration), Phys. Rev. D **90**, 072011 (2014).
[48] ATLAS Collaboration, Report No. ATLAS-CONF-2013-078.
[49] ATLAS Collaboration, Report Nos. ATLAS-CONF-2012-057 and ATLAS-COM-CONF-2012-060 (2012).
[50] S. Chatrchyan *et al.* (CMS Collaboration), Phys. Lett. B **717**, 129 (2012).
[51] S. Chatrchyan *et al.* (CMS Collaboration), J. High Energy Phys. 04 (2014) 191.
[52] CMS Collaboration, Report No. CMS-PAS-TOP-12-033.
[53] T. A. Aaltonen *et al.* (CDF Collaboration, D0 Collaboration), Phys. Rev. D **89**, 072001 (2014).
[54] ATLAS Collaboration, Report Nos. ATLAS-CONF-2012-024 and ATLAS-COM-CONF-2012-009 (2012).
[55] ATLAS Collaboration, Report No. ATLAS-CONF-2013-097.
[56] ATLAS Collaboration, Report No. CMS-PAS-TOP-11-024.
[57] S. Chatrchyan *et al.* (CMS Collaboration), J. High Energy Phys. 02 (2014) 024.
[58] W. Bernreuther and Z.-G. Si, Phys. Rev. D **86**, 034026 (2012).
[59] M. Czakon, M. L. Mangano, A. Mitov, and J. Rojo, J. High Energy Phys. 07 (2013) 167.
[60] J. H. Kuhn and G. Rodrigo, Phys. Rev. Lett. **81**, 49 (1998).
[61] J. H. Kuhn and G. Rodrigo, Phys. Rev. D **59**, 054017 (1999).
[62] J. H. Kuhn and G. Rodrigo, J. High Energy Phys. 01 (2012) 063.

[63] V. Ahrens, A. Ferroglia, M. Neubert, B. D. Pecjak, and L. L. Yang, Phys. Rev. D **84**, 074004 (2011).
[64] A. V. Manohar and M. Trott, Phys. Lett. B **711**, 313 (2012).
[65] W. Hollik and D. Pagani, Phys. Rev. D **84**, 093003 (2011).
[66] P. M. Nadolsky, H.-L. Lai, Q.-H. Cao, J. Huston, J. Pumplin, D. Stump, W.-K. Tung, and C.-P. Yuan, Phys. Rev. D **78**, 013004 (2008).
[67] J. Alwall, M. Herquet, F. Maltoni, O. Mattelaer, and T. Stelzer, J. High Energy Phys. 06 (2011) 128.
[68] M. I. Gresham, I. -W. Kim, and K. M. Zurek, Phys. Rev. D **83**, 114027 (2011).
[69] S. Jung, A. Pierce, and J. D. Wells, Phys. Rev. D **83**, 114039 (2011).
[70] T. Aaltonen *et al.*, Phys. Rev. Lett. **111**, 031802 (2013).
[71] M. J. D. Powell, Acta Numer. **7**, 287 (1998).
[72] M.-x. Luo, H.-w. Wang, and Y. Xiao, Phys. Rev. D **67**, 065019 (2003).
[73] P. Hung and C. Xiong, Nucl. Phys. **B848**, 288 (2011).
[74] G. Aad *et al.* (ATLAS Collaboration), Eur. Phys. J. C **73**, 2261 (2013).
[75] ATLAS Collaboration, Report No. CMS-PAS-TOP-12-027 (2012).
[76] J. Aguilar-Saavedra and M. Perez-Victoria, J. High Energy Phys. 05 (2011) 034.
[77] T. Aaltonen *et al.* (CDF Collaboration), Phys. Rev. D **79**, 112002 (2009).
[78] S. Chatrchyan *et al.* (CMS Collaboration), Phys. Rev. D **87**, 114015 (2013).
[79] V. Abazov *et al.* (D0 Collaboration), Phys. Rev. Lett. **103**, 191803 (2009).
[80] S. Chatrchyan *et al.* (CMS Collaboration), J. High Energy Phys. 05 (2012) 055.
[81] Z. Nagy, Phys. Rev. Lett. **88**, 122003 (2002).
[82] Z. Nagy, Phys. Rev. D **68**, 094002 (2003).
[83] S. Chatrchyan *et al.* (CMS Collaboration), Phys. Rev. Lett. **110**, 141802 (2013).
[84] G. Aad *et al.* (ATLAS Collaboration), Eur. Phys. J. C **73**, 2263 (2013).
[85] T. Aaltonen *et al.* (CDF Collaboration), Phys. Rev. Lett. **108**, 211805 (2012).
[86] S. Chatrchyan *et al.* (CMS Collaboration), Phys. Lett. B **717**, 351 (2012).
[87] G. Aad *et al.* (ATLAS Collaboration), Phys. Rev. D **86**, 091103 (2012).
[88] CMS Collaboration, Report No. CMS-PAS-TOP-12-006.
[89] S. Chatrchyan *et al.* (CMS Collaboration), Phys. Rev. Lett. **110**, 022003 (2013).
[90] ATLAS Collaboration, Report No. ATLAS-CONF-2013-100.
[91] G. Aad *et al.* (ATLAS Collaboration), J. High Energy Phys. 12 (2012) 086.
[92] S. Chatrchyan *et al.* (CMS Collaboration), Phys. Lett. B **730**, 193 (2014).
[93] ATLAS Collaboration, Report No. ATLAS-CONF-2013-091.
[94] W. Grimus, L. Lavoura, O. Ogreid, and P. Osland, J. Phys. G **35**, 075001 (2008).
[95] M. I. Gresham, I.-W. Kim, S. Tulin, and K. M. Zurek, Phys. Rev. D **86**, 034029 (2012).
[96] V. Dzuba, J. Berengut, V. Flambaum, and B. Roberts, Phys. Rev. Lett. **109**, 203003 (2012).
[97] S. Knapen, Y. Zhao, and M. J. Strassler, Phys. Rev. D **86**, 014013 (2012).
[98] W. Bruckner *et al.*, Z. Phys. A **335**, 217 (1990).
[99] G. Erkol, R. Timmermans, and T. Rijken, Phys. Rev. C **74**, 045201 (2006).
[100] D. Akerib *et al.* (LUX Collaboration), Phys. Rev. Lett. **112**, 091303 (2014).
[101] C. McNeile, C. Davies, E. Follana, K. Hornbostel, and G. Lepage, Phys. Rev. D **86**, 074503 (2012).
[102] R. Aaij *et al.* (LHCb collaboration), Phys. Rev. Lett. **112**, 091802 (2014).
[103] J. J. Dudek, R. G. Edwards, P. Guo, and C. E. Thomas (Hadron Spectrum), Phys. Rev. D **88**, 094505 (2013).
[104] M. Neubert, arXiv:hep-ph/9610266.
[105] N. Brambilla *et al.*, Eur. Phys. J. C **74**, 2981 (2014)